



ELSEVIER

Contents lists available at ScienceDirect

## Journal of Theoretical Biology

journal homepage: [www.elsevier.com/locate/jtbi](http://www.elsevier.com/locate/jtbi)

## Bridging short- and long-distance dispersal in individual animal movement

Danish A. Ahmed <sup>a,\*</sup>, Sergei V. Petrovskii <sup>b</sup>, Joseph D. Bailey <sup>c</sup>, Michael B. Bonsall <sup>d</sup>,  
Phillip J. Haubrock <sup>e,f</sup>

<sup>a</sup> CAMB, Center for Applied Mathematics and Bioinformatics, Department of Mathematics and Natural Sciences, Gulf University for Science and Technology, Kuwait

<sup>b</sup> School of Computing and Mathematical Sciences, University of Leicester, UK

<sup>c</sup> School of Mathematics, Statistics and Actuarial Science, University of Essex, Colchester, UK

<sup>d</sup> Department of Biology, University of Oxford, Oxford, OX1 2DL, UK

<sup>e</sup> University of South Bohemia in České Budějovice, Faculty of Fisheries and Protection of Waters, South Bohemian Research Centre of Aquaculture and Biodiversity of Hydrocenoses, Zátěš 728/II, 389 25, Vodňany, Czech Republic

<sup>f</sup> Department of Life and Environmental Sciences, Faculty of Science and Technology, Bournemouth University, Poole, Dorset, UK

## ARTICLE INFO

## Keywords:

Animal movement  
Random walks  
Individual based modelling  
Brownian motion  
Lévy walks  
Dispersal kernels

## ABSTRACT

Random walks (RW) provide a useful modelling framework for the movement of animals at an individual level. If the RW is uncorrelated and unbiased such that the direction of movement is completely random, the dispersal is characterised by the statistical properties of the probability distribution of step lengths, or the dispersal kernel. Whether an individual exhibits short- or long-distance dispersal can be distinguished by the rate of asymptotic decay in the end-tail of the distribution of step-lengths. If the decay is exponential or faster, referred to as a thin-tail, then the step length variance is finite – as occurs in Brownian motion. On the other hand, inverse power-law step length distributions have a heavy end-tail with slower decay, resulting in an infinite step length variance, which is the hallmark of a Lévy walk. In theoretical studies of individual animal movement, various approaches have been employed to connect these dispersal mechanisms, yet they are often ad hoc. We provide a more robust method by ensuring that the survival probability, that is the probability of occurrence of steps longer than a certain threshold is the same for both distributions. Furthermore, the dispersal kernels are then standardised by adjusting the probability to minimise disparities between these distributions. By assuming the same survival probability for movement paths with commonly used thin- and heavy-tailed step length distributions, we form a relationship between the short- and long-distance dispersal of animals in different spatial dimensions. We also demonstrate how our findings can be applied in different ecological contexts, to relate dispersal kernels within theoretical models for boundary effects and spatio-temporal population dynamics. Moreover, we show that the relationship between these dispersal kernels can drastically affect the outcomes across various ecological scenarios.

## 1. Introduction

Understanding the dispersal mechanisms that drive animal movement over multi-spatial scales from local scale foraging and home range exploration to large scale migration, has been a key research focus for ecologists (Bullock et al., 2002; Clobert et al., 2001; Nathan et al., 2008). The virtual ecologist approach where simulations can be used to mimic the movement of real species provides a framework to study fundamental aspects of animal behaviour and movement in a controlled setting (Zurell et al., 2010). Simulating random walks (RW) allows researchers to gain insights into various aspects such as foraging strategies, searching patterns, and movement decisions (Bartumeus et al., 2005; Bartumeus and Catalan, 2009; James et al., 2011; Viswanathan et al.,

2011). It also helps understand how animals respond to specific cues or stimuli (Reynolds, 2010), as well as their navigation and exploration behaviours in their environment (Codling and Bode, 2016; Bailey et al., 2018). Moreover, by incorporating RW models into larger ecological frameworks, in combination with other approaches, such as GPS tracking (Cagnacci et al., 2010; Williams et al., 2020) and individual-based modelling (Grimm and Railsback, 2005), researchers can analyse the causes and consequences of movement dispersal on spatial dynamics (Bowler and Benton, 2005; Hooten et al., 2017).

While several mathematical models have been developed to describe the movement dispersal of animals, on an individual level much of the commonly used methodology is derived from discrete-time random walks (Berg, 1983; Turchin, 1998; Codling et al., 2008). For this, an

\* Corresponding author.

E-mail address: [ahmed.d@gust.edu.kw](mailto:ahmed.d@gust.edu.kw) (D.A. Ahmed).

<https://doi.org/10.1016/j.jtbi.2025.112227>

Received 2 May 2025; Received in revised form 18 July 2025; Accepted 21 July 2025

Available online 29 July 2025

0022-5193/© 2025 The Authors. Published by Elsevier Ltd. This is an open access article under the CC BY license (<http://creativecommons.org/licenses/by/4.0/>).

animal's continuous movement path is mapped as a time-series of distinct locations (Turchin, 1998; Grimm and Railsback, 2005), and the discretised movement path is characterised by the probability distributions of step lengths  $\lambda(l)$  and turning angles. If the RW is uncorrelated and unbiased as occurs in Brownian motion, an individual is equally likely to move in each possible direction with no long-term preferred movement direction, and thus movement dispersal solely relies on the statistical properties of  $\lambda(l)$  (Lin and Segel, 1974; Okubo, 1980). If the step-length distribution is thin-tailed, that is, the end-tail decays sufficiently fast at long step lengths, then the step length variance exists and is finite, and the RW is classed as scale-specific. A direct consequence is that the mean-squared displacement (MSD) is well-defined (i.e., the expected value of the squared beeline distance between an individual's initial and final positions), which is a key metric to analyse movement paths and can be expressed as an exact formula in terms of the number of steps in the walk and the mean-squared step length (Kareiva and Shigesada, 1983). Therefore, any two scale-specific RWs that are parametrised differently can be related by assuming equal MSD (Ahmed et al., 2021b).

A specific example of a movement process that has a thin-tailed dispersal kernel is Brownian motion. Ecologists have routinely applied Brownian motion and diffusive dispersal as a null model for animal movement (Skellam, 1973; Kareiva and Shigesada, 1983), with empirical support found in particular for animals moving in resource-rich environments (Bartumeus et al., 2003; De Knecht et al., 2007; Humphries et al., 2010, 2012; Nolet and Mooij, 2002). Also, a more mechanistic approach to the application of Brownian motion in ecological studies has been emphasised, specifically when resources are abundant. In such cases, Brownian motion has been shown to emerge from ecological interactions rather than being considered a default or primary movement pattern (De Jager et al., 2014).

Another conceptual tool used to model animal movement paths is the Lévy walk (LW) (Viswanathan et al., 2000; Benhamou, 2007; James et al., 2011; Reynolds, 2018). In this case, the end-tail of the step-length distribution decays asymptotically according to an inverse power law,  $\lambda(l) \sim l^{-\mu}$ ,  $1 < \mu < 3$  with slower decay for smaller  $\mu$ , which is referred to as a heavy or fat-tail (Petrovskii and Morozov, 2009). The exponent  $\mu$  determines the type of movement, where  $1 < \mu < 3$  corresponds to a Lévy walk with infinite step-length variance, and  $\mu \geq 3$  is known to converge (albeit slowly) to Brownian motion in the large-step limit (Petrovskii et al., 2014). The corresponding walk has an infinite step length variance and, being scale-free, is self-similar at various spatial scales (Viswanathan et al., 2000; Reynolds, 2018). The movement path is composed of multiple short steps in clusters with the occasional longer steps in between them, resulting in long-distance dispersal since the movement pattern is much faster than Brownian motion. Because of the infinite step length variance, the expected MSD does not exist, and therefore it is less clear how a LW and a scale-specific RW can be related, although a characteristic length scale can always be defined either through the median step length, using geometric-averages, or through dimensional analysis (Kawai and Petrovskii, 2012). Determining whether an animal's movement trajectory can be effectively characterised by a Lévy walk using observed movement data relies on detecting an inverse power law in the survival distribution of step lengths, i.e., the cumulative frequency of lengths greater than any given threshold (Benhamou, 2007). This approach has been adopted in animal movement studies aiming to establish connections between Lévy walks and scale-specific random walks. However, in theoretical contexts where empirical movement data is lacking, an alternative method is needed to relate these different movement processes.

Scale-specific and scale-free movement processes can be related by ensuring that the probability  $p$  of occurrence of steps  $l$  longer than  $L$  is the same for both walks, such that  $\mathbb{P}(l > L) = p$ , henceforth referred to as the 'survival' probability. This terminology is standard in movement ecology and statistical descriptions of heavy-tailed distributions (Benhamou, 2007). To elucidate the rationale for our study, we first outline

several studies that have used this approach across various ecological contexts.

- (i) Bearup et al. (2016) analysed the walking behaviour of *Tenebrio molitor* beetles, where individuals were released into a non-confined circular arena with a central pitfall trap, across repeated experimental trials. During their movement, the beetles approached either the arena's edge or the pitfall trap resulting in falls, and these boundary counts, and the corresponding timing of these crossings were monitored. Individual-based simulations were conducted to replicate the experimental set-up and model various patterns of individual movement. Brownian and Lévy-type movement processes were related with the same characteristic displacement  $L$ , with the same probability fixed at  $p = 0.1$  to leave the arena over a given time interval. This choice was based on empirical observations showing that boundary counts within the first minute consistently accounted for approximately 10% of the total beetle population.
- (ii) Choules and Petrovskii (2017) analysed whether movement patterns quantified by a power-law distribution of movement steps are 'faster' or more 'efficient' than Brownian motion. Counter-intuitively they showed that this comparison depends critically on the relationship between the distributions of step-lengths. Two distinct scale-specific movement processes were related using different approaches, by equating the mean, mean-squared distance or variance of step-lengths. However, in scenarios involving a heavy-tailed distribution where these metrics do not exist, a relation to a thin-tailed distribution was formed based on ensuring equal survival probabilities  $p$  of values 0.1, 0.5, or 0.9. The ecological context provided was that in the case of a natural reserve or protected area,  $p$  is the acceptable risk that a dispersing animal will exit a safe zone of size  $L$ .
- (iii) Ellis et al. (2018) explored the impact of density-dependent individual movement on spatial population distribution within 1D space. They demonstrated that the 'auto-taxis' effect, where individual random walkers adjust their movement based on local density, resulted in a highly heterogeneous population distribution characterised by distinct clusters or patches of animals. Furthermore, across a large spatial domain, the properties of these clusters differed significantly between populations of Brownian and Lévy walkers. The study involved establishing a relationship between the two movement processes, linking a (thin-tailed) normal distribution with a (heavy-tailed) power-law distribution. This ensured that the probability for an animal to remain within a domain over a specified interval was the same across both types of walkers, albeit set hypothetically at 0.9 – corresponding to a survival probability of leaving the domain set at 0.1. The sensitivity of the study's outcomes to this chosen survival probability remains unclear.

With this background, in theoretical studies modelling individual animal movement, there is often a connection made between thin- and heavy-tailed dispersal kernels through an arbitrarily chosen survival probability  $p$ . This choice is typically made for convenience or with limited ecological justification. However, we propose a more rigorous approach, by minimising the dissimilarity between the thin- and heavy-tailed dispersal kernels to establish a fair comparison. This involves determining an optimal value of  $p$  that standardises the dispersal kernels by minimising the squared Euclidean distance between them. This optimisation method provides a clear and interpretable metric for comparing the dispersal kernels, directly accounting for dissimilarities in shape and scale. It ensures an ecologically meaningful relationship between the kernels by balancing the differences in the distributions' tails, and thus provides a robust linkage between short- and long-distance dispersal behaviours. While our approach can also be applied to two scale-specific or two scale-free random walks, our focus is on comparing scale-specific with scale-free processes because these movement models exhibit fundamentally different end-tail behaviours, which is more ecologically relevant. By adopting this methodological refinement,

researchers can achieve a clearer understanding of how different dispersal strategies contribute to population dynamics and spatial distribution patterns in ecological systems. This approach not only enhances theoretical coherence but also strengthens the ecological relevance of modelling individual animal movements.

## 2. Connecting short- and long-distance dispersal in different spatial dimensions

### 2.1. Movement in 1D space

We begin by considering an individual performing a RW in an isotropic environment in one-dimensional (1D) space. Such a modelling framework provides a conceptual basis and thus is useful for developing more realistic ecological models that depict movement phenomena in higher dimensions (Viswanathan et al., 2011; Ellis et al., 2018). If the individual is located at  $x_{i-1}$ , then the location  $x_i$  at the next step is determined by

$$x_i = x_{i-1} + \Delta x_i, \quad i = 1, 2, 3, \dots \quad (2.1)$$

where  $\Delta x_i$  is a random variable for the  $i$ th step along the walk with centrally symmetric probability distribution  $\phi(\Delta x)$  with zero mean  $\mathbb{E}[\Delta x] = 0$ . In this case, moving either to the left or right is equiprobable with value  $1/2$ . The probability of executing a step that exceeds a fixed finite distance  $L$  from the individuals current location  $x_i$  is given by

$$\mathbb{P}(|\Delta x| > L) = p, \quad (2.2)$$

where  $p$  is the survival probability that lies between 0 and 1. Here, we examine two different types of movement that distinguish between short- and long-distance dispersal. The first type has a thin-tailed step distribution characterised by a scale parameter  $\sigma$  and finite step-length variance, denoted as  $\phi_A(\Delta x|\sigma)$ . The second type exhibits a heavy-tailed distribution with a scale parameter  $\gamma$  and infinite variance, represented by  $\phi_B(\Delta x|\gamma)$ . The subscripts  $A$  and  $B$  are used to differentiate between these probability distributions.

Assuming that the survival probability  $p$  is the same for both distributions, we have that:

$$\int_{|\Delta x|>L} \phi_A(\Delta x|\sigma) d\Delta x = \int_{|\Delta x|>L} \phi_B(\Delta x|\gamma) d\Delta x = p, \quad (2.3)$$

and due to symmetry, this can be written as

$$\int_L^\infty \phi_A(\Delta x|\sigma) d\Delta x = \int_L^\infty \phi_B(\Delta x|\gamma) d\Delta x = \frac{p}{2}. \quad (2.4)$$

For commonly used step distributions in simulating animal movements in 1D space, these integrals can be evaluated analytically. In certain scenarios, by eliminating  $L$ , it is possible to express the ratio of distribution parameters as a function of  $p$ , such that

$$\frac{\gamma}{\sigma} = s(p), \quad (2.5)$$

e.g., see later in Section 3.1. We compute the sum of the squared differences between the probability distributions over their domain, using the squared Euclidean distance (i.e.,  $\mathbb{L}^2$ -distance metric), denoted as  $\mathfrak{D}(\phi_B, \phi_A)$  which is given by:

$$\mathfrak{D}(\phi_B, \phi_A) = \int_{-\infty}^\infty [\phi_B(\Delta x|\gamma) - \phi_A(\Delta x|\sigma)]^2 d\Delta x, \quad (2.6)$$

and since these step distributions are centrally symmetric, this can be written as

$$\mathfrak{D}(\phi_B, \phi_A) = 2 \int_0^\infty [\phi_B(\Delta x|\sigma s(p)) - \phi_A(\Delta x|\sigma)]^2 d\Delta x, \quad (2.7)$$

which is expressed solely in terms of  $\sigma$  and  $p$ . To determine the optimal probability  $p^*$  we minimise the  $\mathbb{L}^2$ -distance between these probability distributions, by solving

$$\frac{d\mathfrak{D}}{dp} = 0 \quad (2.8)$$

evaluated at  $p = p^*$ . Minimising the Euclidean distance between two probability distributions is preferred here over other approaches, such as applying the Kolmogorov-Smirnov distance because it directly measures the point-wise differences in probability values, providing a more granular assessment of similarity that is sensitive to exact values at specific points rather than focusing solely on the overall shape of the distributions. Following this, the distribution parameters can be related from Eq. (2.5) as  $\gamma = s(p^*)\sigma$  with corresponding optimal characteristic scale length  $L^*$  from Eq. (2.4).

### 2.2. Movement in 2D space

For the more realistic case of individual movement in two-dimensional (2D) space, e.g., terrestrial animals (Bartumeus et al., 2005; Gurarie and Ovaskainen, 2013; Ahmed et al., 2023), the movement path can be considered as a continuous curvilinear trajectory  $\mathbf{x}(t) = (x(t), y(t))$  over time  $t$ . This movement path can be discretised over time as a series of steps linking an animal's location  $\mathbf{x}_{i-1} = (x_{i-1}, y_{i-1})$  at time  $t_{i-1}$  to the next location  $\mathbf{x}_i = (x_i, y_i)$  at time  $t_i$  as

$$\mathbf{x}_i = \mathbf{x}_{i-1} + (\Delta \mathbf{x})_i, \quad i = 1, 2, 3, \dots \quad (2.9)$$

where  $(\Delta \mathbf{x})_i = (\Delta x_i, \Delta y_i)$  is a step vector whose components are random variables, for the  $i$ th step along the walk, the distances between any two locations are step lengths  $l_i = |\mathbf{x}_i - \mathbf{x}_{i-1}|$ , and  $t_i = i\Delta t$  where  $\Delta t$  is a constant time increment.

In 2D it is more convenient to describe the RW in polar co-ordinates by expressing the step vector in terms of step lengths  $l$  and step orientations  $\theta$  (or headings), using the transformation

$$\Delta x = l \cos \theta, \quad \Delta y = l \sin \theta, \quad l \geq 0, \quad -\pi < \theta \leq \pi \quad (2.10)$$

with inverse transformation

$$l^2 = (\Delta x)^2 + (\Delta y)^2, \quad \theta = \text{atan}_2(\Delta y, \Delta x), \quad (2.11)$$

where  $\text{atan}_2(\Delta y, \Delta x) = \arctan\left(\frac{\Delta y}{\Delta x}\right)$  for  $\Delta x > 0$  and  $\arctan\left(\frac{\Delta y}{\Delta x}\right) \pm \pi$  for  $\Delta x < 0$ . Here,  $\mathbb{E}[l]$  is the mean step length and  $\mathbb{E}[v] = \mathbb{E}[l]/\Delta t$  is the mean speed. The turning angle  $\alpha_i$  can then be measured as the difference between the orientations of two successive steps

$$\alpha_i = \theta_i - \theta_{i-1}. \quad (2.12)$$

On assuming that step lengths  $l_i$  and step orientations  $\theta_i$  are neither autocorrelated nor cross-correlated (Benhamou, 2006), the individual movement can be simulated once the distributions of step lengths  $\lambda(l)$  and turning angles  $\omega(\alpha)$  are prescribed. Since our focus is on movement dispersal arising from the properties of  $\lambda(l)$ , we assume there is no preferred local or global movement direction, resulting in completely random movement and thus  $\alpha$  is uniformly distributed from  $-\pi$  to  $\pi$ , as has been observed in various species (Kareiva, 1983; Hapca et al., 2009; De Jager et al., 2012). Fig. 1 illustrates how an animals' continuous movement path can be described by a random walk, as a series of discrete steps with step-lengths  $l$  and turning angles  $\alpha$ .

Now consider two distinct movement types, the first characterised by a thin-tailed step length distribution  $\lambda_A(l|\sigma)$  with scale parameter  $\sigma$  and finite variance, and second, with a heavy-tailed step length distribution  $\lambda_B(l|\gamma)$  with scale parameter  $\gamma$  and infinite variance. Since step lengths are non-negatively defined, the survival probability is defined as

$$\mathbb{P}(l > L) = p, \quad (2.13)$$

and on fixing  $p$  to be the same for both distributions, one gets

$$\int_L^\infty \lambda_A(l|\sigma) dl = \int_L^\infty \lambda_B(l|\gamma) dl = p. \quad (2.14)$$

The rest of the methodological details are the same as in the 1D case in Section 2.1, where the optimal survival probability  $p^*$  is sought, by minimizing the following  $\mathbb{L}^2$ -distance between the step length probability distributions

$$\mathfrak{D}(\lambda_B, \lambda_A) = \int_0^\infty [\lambda_B(l|\sigma s(p)) - \lambda_A(l|\sigma)]^2 dl \quad (2.15)$$

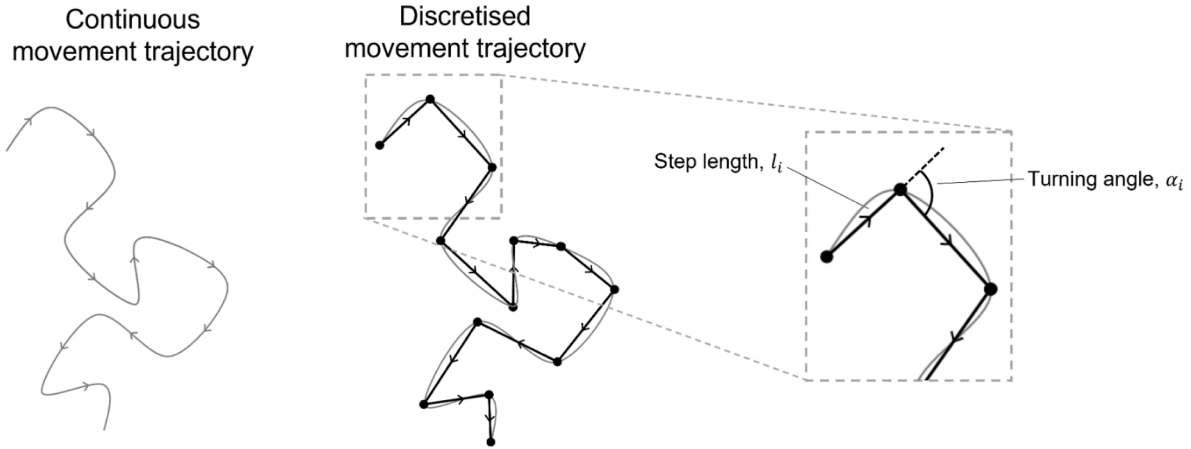


Fig. 1. Mapping the continuous movement trajectory of an animal as a series of discrete steps with step lengths  $l_i$  and turning angles  $\alpha_i$  resulting in the random walk, reproduced from Ahmed et al. (2023).

with relation between distribution parameters  $\gamma = s(p^*)\sigma$  and corresponding optimal characteristic scale length  $L^*$  from Eq. (2.14).

### 2.3. Movement in 3D space

Many animals make use of space in three-dimensions (3D), such as flying and aquatic animals (Cooper et al., 2014; Cleasby et al., 2015; Aspillaga et al., 2019), as well as some ground-dwelling animals that can move through different altitudes on steep terrains (Tracey et al., 2014). In this case, the discrete-time RW model described by Eq. (2.9) applies but extended to 3D by including a vertical direction  $z_i$ , where an animal executes a step by moving from its current location  $\mathbf{x}_{i-1} = (x_{i-1}, y_{i-1}, z_{i-1})$  to the next  $\mathbf{x}_i = (x_i, y_i, z_i)$ , with step lengths between two successive locations  $l_i = |\mathbf{x}_i - \mathbf{x}_{i-1}|$  and random step vector  $(\Delta \mathbf{x})_i = (\Delta x_i, \Delta y_i, \Delta z_i)$ . Using spherical co-ordinates, the step vector can be expressed in terms of step lengths  $l$ , azimuthal angle  $\theta$  which is equivalent to longitude and the polar angle  $\xi$  which is equivalent to co-latitude, using the transformation

$$\begin{aligned} \Delta x &= l \cos(\theta) \sin(\xi), & \Delta y &= l \sin(\theta) \sin(\xi), & \Delta z &= l \cos(\xi), \\ l &\geq 0, & -\pi &< \theta \leq \pi, & 0 &\leq \xi \leq \pi \end{aligned} \quad (2.16)$$

with inverse transformation

$$l = \sqrt{(\Delta x)^2 + (\Delta y)^2 + (\Delta z)^2}, \quad \theta = \text{atan}_2(\Delta y, \Delta x), \quad \xi = \arccos\left(\frac{\Delta z}{l}\right). \quad (2.17)$$

In an isotropic environment,  $\theta$  is uniformly distributed from  $-\pi$  to  $\pi$ , and  $\xi$  is half-sine distributed  $\frac{1}{2} \sin(\xi)$  with values drawn between 0 and  $\pi$  (Ahmed et al., 2021). Thus in this case, the movement pattern is characterised by the distribution of step lengths  $\lambda(l)$ . A relationship between short- or long-distance dispersal in 3D can be obtained using the methodology described in 2D, see Section 2.2, with the survival probability given by Eq. (2.13), which is optimised by minimising the  $\mathbb{L}^2$ -distance in Eq. (2.15).

## 3. Connecting short- and long-distance dispersal for $\mu = 2$

### 3.1. Normal and Cauchy step distributions (1D case)

To relate two distinct RWs in 1D, we consider steps to be independently Gaussian (normally) distributed  $\phi_G$  which is given as

$$\phi_G(\Delta x|\sigma) = \frac{1}{\sigma\sqrt{2\pi}} \exp\left(-\frac{(\Delta x)^2}{2\sigma^2}\right), \quad (3.1)$$

with zero mean  $\mathbb{E}[\Delta x] = 0$  and finite variance  $\sigma^2$ . This distribution is thin-tailed due to the faster than exponential decay in the end tails. Alongside this, consider the Cauchy step distribution  $\phi_C$ , which reads

$$\phi_C(\Delta x|\gamma) = \frac{\gamma}{\pi(\gamma^2 + (\Delta x)^2)}, \quad (3.2)$$

which is heavy-tailed due to the slower decay in the end tails according to  $\phi_C \sim \frac{1}{(\Delta x)^2}$  as  $|\Delta x| \rightarrow \infty$ , with infinite variance. For these distributions, we can express the characteristic scale length  $L$  in terms of the survival probability  $p$  by applying Eq. (2.4),

$$\int_L^\infty \phi_G(\Delta x|\sigma) d\Delta x = \int_L^\infty \phi_C(\Delta x|\gamma) d\Delta x = \frac{p}{2} \quad (3.3)$$

which gives

$$L = \sigma\sqrt{2}\text{erfc}^{-1}(p) = \gamma \tan\left[\frac{\pi(1-p)}{2}\right] \quad (3.4)$$

where  $\text{erfc}^{-1}(\tau)$  is the inverse of the complimentary error function defined by  $\text{erfc}(\tau) = \frac{2}{\sqrt{\pi}} \int_\tau^\infty \exp(-t^2) dt$ . On rearranging the above equation, we can express the ratio of distribution parameters as a function of  $p$  only:

$$s(p) = \frac{\gamma}{\sigma} = \sqrt{2}\text{erfc}^{-1}(p) \cot\left[\frac{\pi(1-p)}{2}\right]. \quad (3.5)$$

The  $\mathbb{L}^2$ -distance is given as

$$\mathfrak{D}(\phi_C, \phi_G) = \frac{1}{\sigma\sqrt{\pi}} \cdot \left[ \frac{1}{s\sqrt{\pi}} - 2\sqrt{2} \exp\left(\frac{s^2}{2}\right) \text{erfc}\left(\frac{s}{\sqrt{2}}\right) + 1 \right], \quad (3.6)$$

where  $s = s(p)$  for brevity. The optimal survival probability  $p^*$  which minimizes this occurs when

$$\frac{d\mathfrak{D}}{dp} = -\frac{s'}{2\pi\sigma\mathfrak{D}} \left[ \frac{1-4s^2}{s^2} + 2\sqrt{2}\pi s \exp\left(\frac{s^2}{2}\right) \text{erfc}\left(\frac{s}{\sqrt{2}}\right) \right] = 0, \quad (3.7)$$

which gives  $p^* = 0.721$ , and is invariant with respect to  $\sigma$ . The distribution parameter ratio is  $s^* = 0.762$  and  $L^* = 0.357\sigma$  from Eq. (3.4).

For movement in 1D space, when examining the Gaussian step distributions depicted in Fig. 2(a) and (b), visually it appears as a subtle distinction. Yet, this change in  $\sigma$  from 0.125 to 0.131 arising from relating the distributions in different ways, can result in a considerable effect on the ensuing movement process. For instance, in Brownian motion with Gaussian increments, the mean-squared displacement (MSD) is given by  $n\sigma^2$ , where  $n$  is the number of steps in the walk. The effect of this change in  $\sigma$  becomes particularly noticeable at larger spatial scales, where the movement is less constrained, and the increased MSD leads to a faster dispersal. In smaller habitats or restricted spaces, however, even a subtle change in  $\sigma$  can have a considerable impact, as the movement

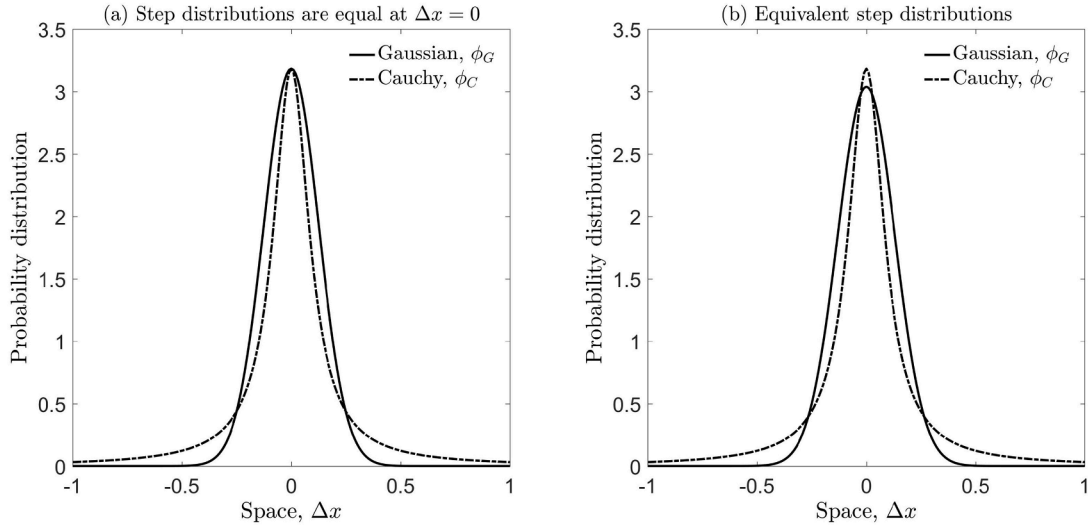


**Fig. 2.** (a) Relationship between the Gaussian (solid) and the Cauchy (dashed) step distributions by ensuring the same peak value at  $\Delta x = 0$ . Here, we set  $\gamma = 0.1$  and compute  $\sigma = \frac{\gamma\sqrt{2\pi}}{2} = 0.125$ . Illustration in (a) adapted from Figure 5.2 in Lutscher (2019), but used therein in the context of dispersal kernels. (b) Gaussian and Cauchy step distributions related using the method outlined in this section, with optimal survival probability  $p^* = 0.721$ , distribution parameter ratio  $s^* = 0.762$ , and for  $\gamma = 0.1$  we have that  $\sigma = \gamma/s^* = 0.131$ . In (b) the Gaussian distribution exhibits a higher frequency of longer steps, rendering it more akin to the Cauchy distribution. This is counterbalanced by a reduced peak.

is confined. Consider, for example, a 1D conceptual scenario of pest insect immigration into a monitored habitat fitted with a trap. The growth patterns in trap counts are influenced not only by the type of boundary – how the insect population outside the habitat moves diffusively and occasionally crosses the habitat boundary – but also by the insects’ dispersal capability (Bearup et al., 2015). The effect of faster dispersal is more realised in case of smaller habitat size, leading to a more rapid accumulation of trap counts.

**3.2. Rayleigh and folded-Cauchy step-length distributions (2D case)**

Consider a 2D RW with random step vector  $(\Delta x) = (\Delta x, \Delta y)$  whose components are independently distributed according to a zero-centered normal distribution  $\phi_G(\Delta x)$  and  $\phi_G(\Delta y)$  with the same finite variance  $\sigma^2$ , see Eq. (3.1). It can be derived that the corresponding step length distribution is the Rayleigh distribution  $\lambda_R$ , which reads

$$\lambda_R(l) = \frac{l}{\sigma^2} \exp\left(-\frac{l^2}{2\sigma^2}\right), \tag{3.8}$$

with mean step length  $\mathbb{E}(l) = \frac{\sigma\sqrt{2\pi}}{2}$  and finite variance  $2\sigma^2\left(1 - \frac{\pi}{4}\right)$ , (Petrovskii et al., 2014). The resulting movement type is a discrete-time model of Brownian motion (Turchin, 1998; Petrovskii et al., 2012). Alternatively, consider a folded-Cauchy step-length distribution  $\lambda_{fC}$ , which reads

$$\lambda_{fC}(l|\gamma) = \frac{2\gamma}{\pi(\gamma^2 + l^2)}, \tag{3.9}$$

with quadratic decay in the end tail according to  $\lambda_{fC} \sim \frac{1}{l^2}$  as  $l \rightarrow \infty$ , with infinite variance. The characteristic scale length  $L$  can be expressed in terms of the survival probability  $p$  to get

$$L = \sigma\sqrt{-2 \ln p} = \gamma \tan\left[\frac{\pi}{2}(1 - p)\right], \tag{3.10}$$

and on rearranging this, the ratio of distribution parameters is

$$s(p) = \frac{\gamma}{\sigma} = \sqrt{-2 \ln p} \cot\left[\frac{\pi}{2}(1 - p)\right]. \tag{3.11}$$

The  $\mathbb{L}^2$ -distance between these step length distributions is

$$\mathfrak{D}(\lambda_{fC}, \lambda_R) = \frac{1}{\pi\sigma} \cdot \left(\frac{1}{s} - 2s \exp\left(\frac{s^2}{2}\right) \text{E}_1\left(\frac{s^2}{2}\right) + \frac{\pi\sqrt{\pi}}{4}\right), \tag{3.12}$$

where  $\text{E}_1(\tau) = \int_{\tau}^{\infty} \frac{1}{t} \exp(-t) dt$  is a form of the exponential integral. The optimal survival probability is a solution of

$$\frac{d\mathfrak{D}}{dp} = -\frac{s'}{2\pi\sigma\mathfrak{D}} \left[ \frac{1 - 4s^2}{s^2} + 2(1 + s^2) \exp\left(\frac{s^2}{2}\right) \text{E}_1\left(\frac{s^2}{2}\right) \right] = 0, \tag{3.13}$$

which gives  $p^* = 0.658$ , with distribution parameter ratio  $s^* = 1.536$  and  $L^* = 0.915\sigma$  from Eq. (3.10).

Fig. 3 illustrates the comparative movement patterns between short- and long-distance dispersal. Panels (a)–(c) depict scenarios with a Rayleigh step length distribution ( $\sigma = 0.5$ ,  $n = 50$  steps), while panels (b)–(d) show scenarios with a folded-Cauchy step length distribution ( $\mu = 2$ ,  $\gamma = s\sigma = 0.768$ ,  $n = 100$  steps). For both distributions, the survival probability  $p^* = 0.658$  of executing step lengths greater than  $L^* = 0.458$  is the same, represented by the fixed radius of the circles. Note that, in the case of long-distance dispersal, it is possible that an individual can execute extremely large steps during its movement, and not necessarily stay within a region of approximately the same size.

**3.3. Chi and folded-Cauchy step-length distributions (3D case)**

For Brownian motion in 3D space the step increments  $(\Delta x) = (\Delta x, \Delta y, \Delta z)$  are independently distributed according to a zero-centered normal distribution with the same finite variance, see Eq. (3.1). In this case the variable  $l/\sigma$  follows a chi distribution with three degrees of freedom, corresponding to step length distribution  $\lambda_{\chi}$ , given as

$$\lambda_{\chi}(l|\sigma) = \frac{2l^2}{\sigma^3\sqrt{2\pi}} \exp\left(-\frac{l^2}{2\sigma^2}\right), \tag{3.14}$$

with mean step length  $\mathbb{E}(l) = 4\sigma/\sqrt{2\pi}$  and finite variance  $3\sigma^2\left(1 - \frac{8}{3\pi}\right)$ , (Ahmed et al., 2021).

If we also consider the folded-Cauchy step length distribution  $\lambda_{fC}$  in Eq. (3.9), the characteristic scale length  $L$  can be related to the survival probability  $p$  as

$$L = \sigma\sqrt{2I^{-1}\left(p, \frac{3}{2}\right)} = \gamma \tan\left[\frac{\pi}{2}(1 - p)\right] \tag{3.15}$$

where  $I^{-1}(\tau, a)$  is the inverse of the upper incomplete gamma function, defined as  $I(\tau, a) = \frac{1}{\Gamma(a)} \int_{\tau}^{\infty} (t')^{a-1} e^{-t'} dt'$ . On re-arranging Eq. (3.15) we

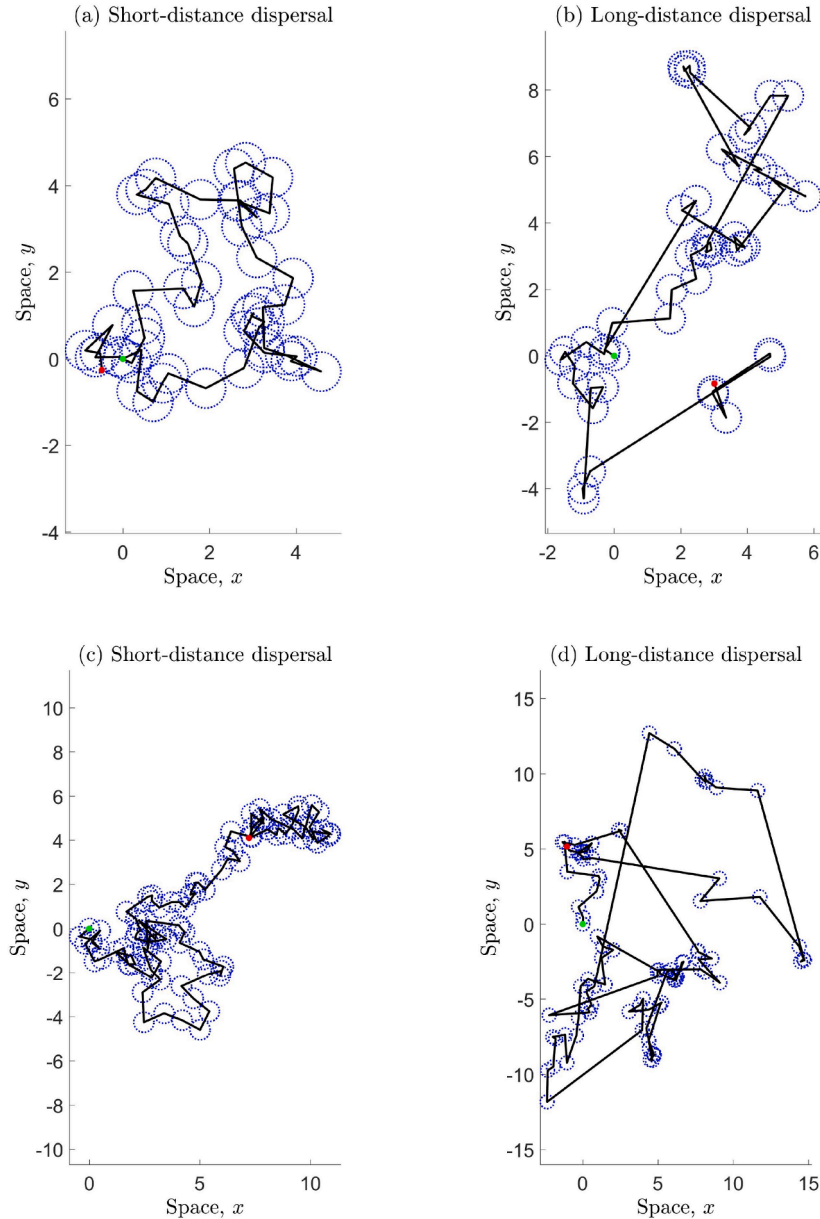


**Fig. 3.** An individual random walker performing short- and long-distance dispersal in 2D space. (a) Brownian motion with Rayleigh distributed step lengths ( $\sigma = 0.5$ ), and (b) LW with folded-Cauchy distributed step-lengths ( $\gamma = 0.768$ ). The ratio of distribution parameters is  $s^* = 1.536$  with optimal survival probability  $p^* = 0.658$ . Both movement processes have the same survival probability  $p^*$ , with the length scale  $L^* = 0.458$  (radius of dashed circles at each location). Each individual starts at the origin (green marker) and the walk terminates after executing  $n = 50$  steps (red marker). Panels (c) and (d) are random walks with the same parametrisation as in (a) and (b), but run for a larger number of  $n = 100$  steps.

have

$$s(p) = \frac{\gamma}{\sigma} = \sqrt{2I^{-1}\left(p, \frac{3}{2}\right) \cot\left[\frac{\pi}{2}(1-p)\right]}. \quad (3.16)$$

We can compute an analytic expression for the  $\mathbb{L}^2$ -distance as

$$\mathfrak{D}(\lambda_{FC}, \lambda_\gamma) = \frac{1}{\sigma\sqrt{\pi}} \cdot \left[ \frac{1-4s^2}{s\sqrt{\pi}} + 2\sqrt{2}s^2 \exp\left(\frac{s^2}{2}\right) \operatorname{erfc}\left(\frac{s}{\sqrt{2}}\right) + \frac{3}{4} \right], \quad (3.17)$$

with optimal survival probability  $p^*$  as a solution of

$$\frac{d\mathfrak{D}}{dp} = -\frac{s'}{2\pi\sigma\mathfrak{D}} \left[ \left(\frac{1}{s} + 2s\right)^2 - 2\sqrt{2}\pi s(2 + s^2) \exp\left(\frac{s^2}{2}\right) \operatorname{erfc}\left(\frac{s}{\sqrt{2}}\right) \right] = 0, \quad (3.18)$$

which gives  $p^* = 0.650$ , with distribution parameter ratio  $s^* = 2.089$ , with  $L^* = 1.282\sigma$  from Eq. (3.15).

#### 4. Connecting short- and long-distance dispersal for general exponent $\mu$

##### 4.1. Normal and power-law step distributions (1D case)

We consider two distinct RWs in 1D space where the probability distributions of the step increments are normally distributed  $\phi_G(\Delta x)$ , and alternatively distributed according to a power law

$$\phi_P(\Delta x|\gamma, \mu) = \frac{A}{(\gamma + |\Delta x|)^\mu}, \quad A = \frac{1}{2}(\mu - 1)\gamma^{\mu-1}, \quad 1 < \mu \leq 3, \quad (4.1)$$

where  $\gamma$  is the distribution scale parameter and  $A$  is a normalisation constant. This is a heavy-tailed distribution with infinite variance, and the

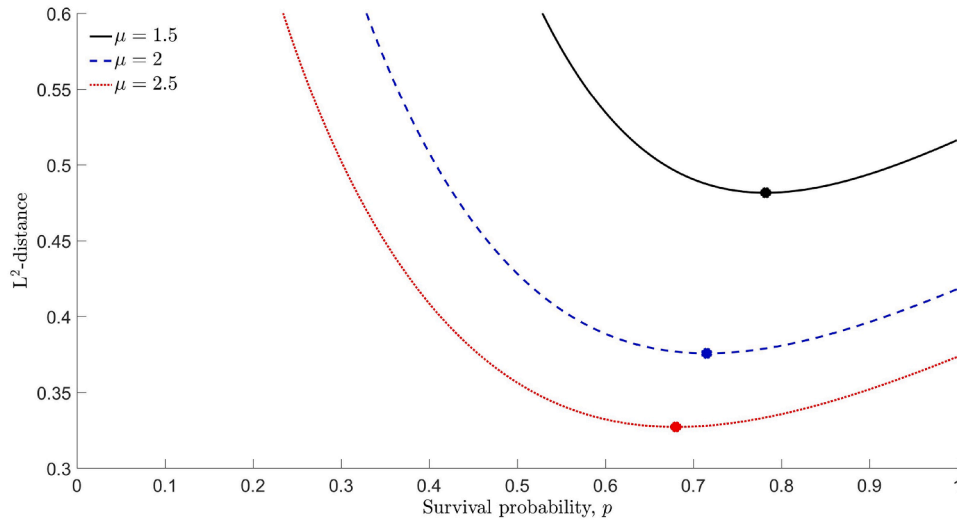


**Fig. 4.** Plot of the  $\mathbb{L}^2$ -distance between the step distributions  $\phi_p$  and  $\phi_G$  with  $\sigma = 0.5$  as a function of the survival probability  $p$ , for different heavy-tail exponents  $\mu = 1.5, 2, 2.5$ . The markers depict the minimum point in each case, that is the optimal probability  $p^*$  at which the  $\mathbb{L}^2$ -distance is minimised  $\mathfrak{D}^*$ . For  $\mu = 1.5$ ,  $\mathfrak{D}^* = 0.482$  at  $p^* = 0.782$ , for  $\mu = 2$ ,  $\mathfrak{D}^* = 0.376$  at  $p^* = 0.715$  and for  $\mu = 2.5$ ,  $\mathfrak{D}^* = 0.327$  at  $p^* = 0.680$ .

rate of decay in the end tails is  $\phi_p \sim \frac{1}{|\Delta x|^\mu}$  as  $|\Delta x| \rightarrow \infty$ , with faster decay for larger exponent  $\mu$ . Applying the condition  $\mathbb{P}(l > L) = p$  for both of these distributions, the characteristic scale length  $L$  can be expressed in terms of the survival probability  $p$  as

$$L = \sigma \sqrt{2} \operatorname{erfc}^{-1}(p) = \gamma \left( p^{\frac{1}{1-\mu}} - 1 \right) \tag{4.2}$$

and on eliminating  $L$  the ratio of distribution parameters is

$$s(p|\mu) = \frac{\gamma}{\sigma} = \frac{\sqrt{2} \operatorname{erfc}^{-1}(p)}{p^{\frac{1}{1-\mu}} - 1}. \tag{4.3}$$

The  $\mathbb{L}^2$ -distance between these probability distributions  $\phi_p$  and  $\phi_G$  is

$$\mathfrak{D}(\phi_p, \phi_G) = \frac{2}{\sigma^2} \int_0^\infty \left[ \frac{\mu - 1}{2s \left(1 + \frac{\Delta x}{\sigma s}\right)^\mu} - \frac{1}{\sqrt{2\pi}} \exp\left(-\frac{(\Delta x)^2}{2\sigma^2}\right) \right]^2 d\Delta x. \tag{4.4}$$

Let  $\zeta = \frac{\Delta x}{\sigma}$ , the integral becomes

$$\mathfrak{D}(\phi_p, \phi_G) = \frac{2}{\sigma} \int_0^\infty \left[ \frac{\mu - 1}{2s \left(1 + \frac{\zeta}{s}\right)^\mu} - \frac{1}{\sqrt{2\pi}} \exp\left(-\frac{\zeta^2}{2}\right) \right]^2 d\zeta. \tag{4.5}$$

The  $\mathbb{L}^2$ -distance is scaled by a factor of  $1/\sigma$ , and therefore decreases with larger  $\sigma$ , but is minimised at some optimal probability  $p^*$  which is independent of  $\sigma$ . This integral is not analytically tractable, but can be evaluated using numerical integration techniques such as the trapezoidal rule. Computed values of  $p^*$  for different values of  $\mu$  are provided in Table 1.

Fig. 4 illustrates that the  $\mathbb{L}^2$ -distance is minimised with optimal probability  $p^* = 0.782$  for  $\mu = 1.5$ ,  $p^* = 0.715$  for  $\mu = 2$ , and  $p^* = 0.680$  for  $\mu = 2.5$ . Therefore  $p^*$  increases with slower asymptotic decay in the end tails. A relationship can be sought between the two movement processes in 1D space with normal and power-law step distributions by relating distribution parameters through the ratios  $s^* = \gamma/\sigma = 0.435, 0.916, 1.407$ , respectively, with corresponding length scales  $L^* = 0.277\sigma, 0.365\sigma, 0.412\sigma$  determined by Eq. (4.2). Furthermore, in Section 3.1, we found a similar approximate value of  $p^* \approx 0.72$  when comparing the normal and Cauchy ( $\mu = 2$ ) probability step distributions. This suggests that, in this scenario, the details of the shape of the heavy-tailed distribution – such as its peak and spread around the central value – does not play a major role in the ensuing movement dynamics, but rather the similarity is attributed to the heaviness of the tail in both distributions.

#### 4.2. Rayleigh and Pareto step-length distributions (2D case)

Consider the movement of two individuals performing a RW in 2D space, with step length distributions given by the Rayleigh distribution  $\lambda_R(l)$  in Eq. (3.8) and a Pareto distribution with general exponent  $\mu$  given by

$$\lambda_P(l|\gamma, \mu) = \frac{A}{(\gamma + l)^\mu}, \quad A = (\mu - 1)\gamma^{\mu-1}, \quad 1 < \mu \leq 3, \tag{4.6}$$

where  $\gamma$  is the distribution parameter and  $A$  is a normalizing constant. The distribution is heavy-tailed with rate of decay  $\lambda_P \sim \frac{1}{l^\mu}$  as  $l \rightarrow \infty$ , and has an infinite variance. Using the definition of the survival probability  $\mathbb{P}(l > L) = p$  for both distributions, we obtain

$$L = \sigma \sqrt{-2 \ln p} = \gamma \left( p^{\frac{1}{1-\mu}} - 1 \right) \tag{4.7}$$

with ratio of distribution parameters

$$s(p|\mu) = \frac{\gamma}{\sigma} = \frac{\sqrt{-2 \ln p}}{p^{\frac{1}{1-\mu}} - 1}. \tag{4.8}$$

The  $\mathbb{L}^2$ -distance between these probability distributions  $\lambda_p$  and  $\lambda_R$  is

$$\mathfrak{D}(\lambda_p, \lambda_R) = \int_0^\infty \left[ \frac{\mu - 1}{\sigma s \left(1 + \frac{l}{\sigma s}\right)^\mu} - \frac{1}{\sigma^2} \exp\left(-\frac{l^2}{2\sigma^2}\right) \right]^2 dl, \tag{4.9}$$

and by introducing a change of variables by re-scaling step lengths  $\zeta = \frac{l}{\sigma}$ , this can be written as

$$\mathfrak{D}(\lambda_p, \lambda_R) = \frac{1}{\sigma} \int_0^\infty \left[ \frac{\mu - 1}{s \left(1 + \frac{\zeta}{s}\right)^\mu} - \zeta \exp\left(-\frac{\zeta^2}{2}\right) \right]^2 d\zeta, \tag{4.10}$$

which decreases with an increase in  $\sigma$ . The optimal probability  $p^*$  which minimises the  $\mathbb{L}^2$ -distance can be computed numerically (Table 1).

#### 4.3. Chi and Pareto step-length distributions (3D case)

For movement in 3D space, consider the following step length distributions, chi  $\lambda_\chi$  in Eq. (3.14) and Pareto  $\lambda_P$  in Eq. (4.6). In this case the characteristic scale length is

$$L = \sigma \sqrt{2I^{-1}\left(p, \frac{3}{2}\right)} = \gamma \left( p^{\frac{1}{1-\mu}} - 1 \right) \tag{4.11}$$

**Table 1**

Optimal survival probabilities  $p^*$  are evaluated by relating Brownian motion to LWs with varying exponents  $\mu$ , across different spatial dimensions.

$\mu$	1D	2D	3D	$\mu$	1D	2D	3D
1.1	0.919	0.908	0.902	2.1	0.707	0.709	0.705
1.2	0.867	0.858	0.852	2.2	0.699	0.702	0.698
1.3	0.831	0.824	0.817	2.3	0.692	0.696	0.692
1.4	0.804	0.798	0.792	2.4	0.686	0.690	0.687
1.5	0.782	0.777	0.772	2.5	0.680	0.686	0.682
1.6	0.764	0.761	0.755	2.6	0.675	0.681	0.677
1.7	0.749	0.747	0.742	2.7	0.670	0.677	0.673
1.8	0.736	0.735	0.730	2.8	0.666	0.673	0.670
1.9	0.725	0.725	0.721	2.9	0.662	0.670	0.666
2.0	0.715	0.717	0.712	3.0	0.658	0.666	0.663

with ratio of distribution parameters

$$s(p|\mu) = \frac{\gamma}{\sigma} = \frac{\sqrt{2I^{-1}\left(p, \frac{3}{2}\right)}}{p^{\frac{1}{1-\mu}} - 1}. \tag{4.12}$$

The  $\mathbb{L}^2$ -distance between  $\lambda_\chi$  and  $\lambda_p$  is

$$\mathfrak{D}(\lambda_\chi, \lambda_p) = \int_0^\infty \left[ \frac{\mu - 1}{\sigma s \left(1 + \frac{l}{\sigma s}\right)^\mu} - \frac{2l^2}{\sigma^3 \sqrt{2\pi}} \exp\left(-\frac{l^2}{2\sigma^2}\right) \right]^2 dl, \tag{4.13}$$

and with re-scaled step lengths  $\zeta = \frac{l}{\sigma}$ , this reads

$$\mathfrak{D}(\lambda_\chi, \lambda_p) = \frac{1}{\sigma} \int_0^\infty \left[ \frac{\mu - 1}{s \left(1 + \frac{\zeta}{s}\right)^\mu} - \frac{2\zeta^2}{\sqrt{2\pi}} \exp\left(-\frac{\zeta^2}{2}\right) \right]^2 d\zeta, \tag{4.14}$$

with optimal probability  $p^*$  that minimises this  $\mathbb{L}^2$ -distance computed numerically (Table 1).

#### 4.4. Optimal survival probability as a function of the heavy-tail exponent

To determine a functional relationship that expresses the survival probability  $p^*$  explicitly in terms of  $\mu$ , we compute  $p^*$  for Brownian motion in different spatial dimensions, considering various LW heavy-tail exponents  $\mu$ . Step length distributions are examined in different scenarios: normal vs. power law in Section 4.1, Rayleigh vs. Pareto in Section 4.2, and chi vs. Pareto in Section 4.3. We find that the values of  $p^*$  are similar across various spatial dimensions (Table 1). This similarity is not coincidental, but rather a numerically verifiable trend, arising from the comparison of different LW movement types to the same underlying Brownian movement process.

We propose an Ansatz function to express  $p^*$  as a function of  $\mu$ ,

$$p^*(\mu) = \frac{c_0(\mu - 1) + 1}{c_1(\mu - 1) + 1}, \quad 1 < \mu \leq 3 \tag{4.15}$$

where  $c_0$  and  $c_1$  are parameters estimated from non-linear regression curve fitting, see Fig. 5 for the case of a LW in 2D space.

Despite the similarity in values of  $p^*$ , on curve-fitting the Ansatz function against values of  $\mu$ , the best-fit model parameters vary, reported in Table 2. In particular, there is an overlap for these parameter estimates in the 2D and 3D cases, where  $c_0$  lies in [1.61, 1.77], and  $c_1$  lies in [2.67, 2.88]. It follows that a reasonable estimate ensuring 99% accuracy are the midpoints of these intervals, giving  $c_0 = 1.7$  and  $c_1 = 2.8$ .

A general observation is that the curve exhibits a non-linear relationship where  $p^*$  decreases with increasing  $\mu$ , that is for heavy end-tail(s) that asymptotically decay at a faster rate (Fig. 5). The Ansatz function serves to approximate the optimal survival probability  $p^*$  required to relate Brownian motion to a LW with power-law distributed step lengths across various spatial dimensions and for a broad range of

**Table 2**

The Ansatz function was fitted to values of  $\mu$ , representing LWs in different spatial dimensions. The non-linear regression curve fitting tool *lsqcurvefit* from Matlab was used to estimate the best-fit model parameters  $c_0, c_1$ , and the 99% confidence intervals (CI) are provided for the range of parameter values. The goodness of fit was assessed using the coefficient of determination  $R^2$  and the root mean square error  $RMSE$ .

Parameter	1D	2D	3D
$c_0$	1.32	1.64	1.77
$c_1$	2.25	2.70	2.90
CI for $c_0$	[1.24, 1.40]	[1.51, 1.77]	[1.61, 1.93]
CI for $c_1$	[2.13, 2.36]	[2.52, 2.88]	[2.67, 3.12]
$R^2$	0.999	0.998	0.997
$RMSE$	0.002	0.003	0.003

exponents  $\mu$ . For instance, for  $\mu = 1.25$ , we compute from Eq. (4.15) that  $p^* \approx 0.851$  for movement in 1D space ( $c_0 = 1.32, c_1 = 2.25$ ), and  $p^* \approx 0.838$  for movement in either 2D or 3D space ( $c_0 = 1.7, c_1 = 2.8$ ). Thus, the functional relationship (Eq. (4.15)) not only makes our approach simpler in practice, but also allows for quick approximation of  $p^*$  for any value of  $\mu$  that lies between 1 and 3, reducing computational effort.

## 5. Ecological applications

### 5.1. Boundary counts

A population of  $N$  individuals is uniformly distributed across a non-confined circular region with radius  $R$ , such that each individual has an equal probability of being located at any point within the region. Individuals in the population move independently either according to Brownian motion, or in another scenario according to a LW, and execute  $n$  steps. The boundary counts, which is the proportion of individuals exiting the region, are recorded at each step of the walk. Fig. 6 illustrates the spatial population distribution and the individuals that remain within the region. Here, the movement types have the same optimal survival probability,  $p^*$ , and are uniquely related by minimising the Euclidean distance between their step-length distributions. After a large number of steps, the boundary counts are much higher for the population executing a LW, as expected due to its longer step lengths compared to Brownian motion.

Fig. 7 shows the boundary counts for scenarios of the population moving according to either Brownian motion (black curve), or a LW (blue curves). The step-length distributions corresponding to these movement processes are related at varying survival probabilities  $p$ , including the optimal value  $p^*$  as computed using our method. It is evident that boundary counts can drastically change, and thus are sensitive to the choice of  $p$ . This sensitivity underscores the importance of carefully selecting how the step-length distributions are to be related. Ideally, this choice should be guided by strong ecological justifications that align with the behaviour of the studied populations. Otherwise, in case where direct ecological insights are limited, the default approach is to use  $p^*$ , which minimises the dissimilarity between the step-length distributions.

### 5.2. Spatio-temporal population dynamics

Integro-difference equations (IDEs) provide a useful modelling framework to describe the spatio-temporal dynamics of a population (Kot and Schaffer, 1986; Andersen, 1991; Neubert et al., 1995), and has advantages over other approaches (e.g., diffusion-reaction models, Holmes et al., 1994; Okubo and Levin, 2001) due to the ability to capture more complex spatial dynamics, non-local interactions, and various dispersal processes.

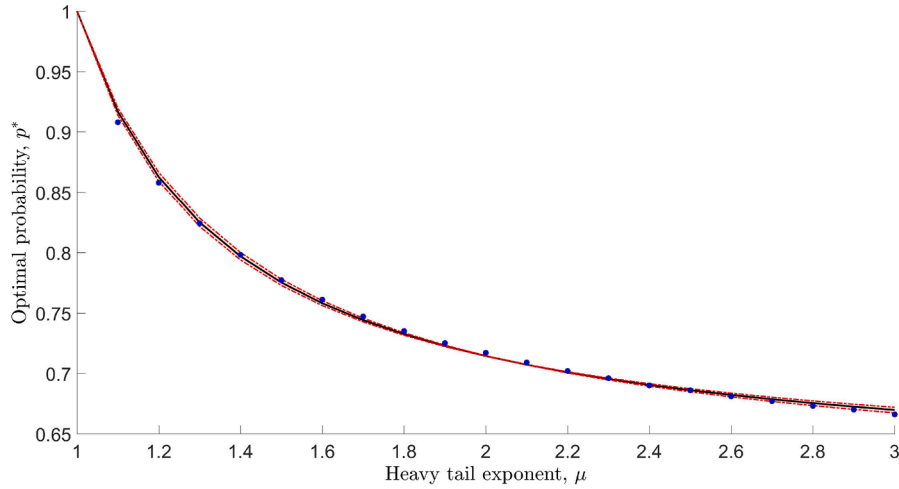


**Fig. 5.** The Ansatz function (solid curve) is fitted to determine optimal probabilities  $p^*$  as a function of the exponent  $\mu$ , illustrated here specifically for the 2D case. The best fit parameters are  $c_0 = 1.64$  and  $c_1 = 2.70$ . The shaded area between the dashed curves represents a 99% confidence region for the parameter values:  $c_0$  ranges from 1.51 to 1.77, and  $c_1$  ranges from 2.52 to 2.88. The goodness of fit is assessed by the coefficient of determination  $R^2 = 0.998$  and the root mean square error  $RMSE = 0.003$ . Refer to Table 2 for details.

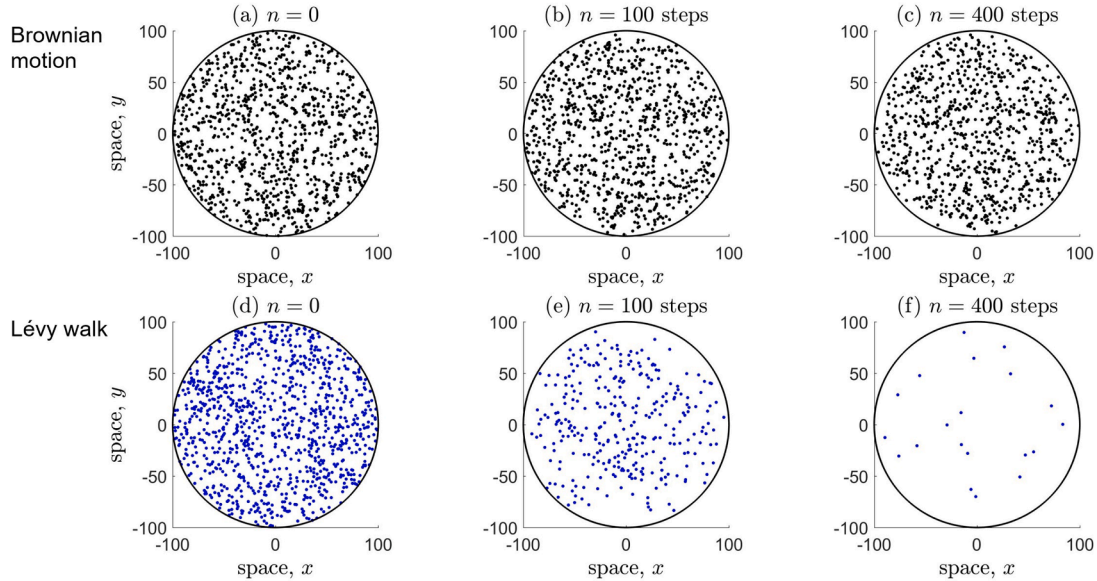


**Fig. 6.** Snapshots of the spatial distribution of two populations within a non-confined circular region of radius  $R = 100$ . The black dots represent 1000 individuals performing Brownian motion with a Rayleigh step-length distribution ( $\sigma = 0.5$ ), while the blue dots depict another 1000 individuals following a LW with a folded-Cauchy step-length distribution ( $\gamma = 0.768$ ). These movement processes are related with the same survival probability  $p^* = 0.658$ , using the method outlined in Section 3.2. Each panel shows the individuals that remain within the circular region after (a)  $n = 0$  steps (initial population distribution), (b)  $n = 100$  steps and (c) 400 steps.

The governing equation reads

$$N_{t+1}(\mathbf{r}) = \int_{\Omega} \lambda(\mathbf{r}, \mathbf{r}') F(N_t(\mathbf{r}')) d\mathbf{r}' \quad (5.1)$$

where  $N_t$  is the population density in year  $t$ ,  $F(\cdot)$  is a growth function that describes the ecological mechanisms and processes that underlie the growth dynamics (Sandefur, 2018), and  $\lambda(\mathbf{r}, \mathbf{r}')$  is the dispersal kernel which gives the probability distribution of the event that an individual located before dispersal at position  $\mathbf{r}' = (x', y')$  moves after dispersal to the position  $\mathbf{r} = (x, y)$  over a dispersal domain  $\Omega$  (Lewis et al., 2006; Lutscher, 2019). Here, our focus is on the rate of spread in the population which depends on the properties of the dispersal kernel. Assuming that dispersal is homogeneous and isotropic so that the probability of moving from  $\mathbf{r}$  to  $\mathbf{r}'$  depends only on the distance  $r$  between the two positions, it follows that  $\lambda(\mathbf{r}, \mathbf{r}') = \lambda(r)$ , where  $r = |\mathbf{r} - \mathbf{r}'| = \sqrt{(x - x')^2 + (y - y')^2}$ . Note that we use a different notation,  $\lambda(r)$ , for the dispersal kernel to

reflect the use of IDEs in modelling animal dispersal, in contrast to the RW framework in earlier sections, where the step-length distribution is denoted by  $\lambda(l)$ . This notation follows standard conventions in the ecological literature (c.f., Benhamou, 2007; Rodrigues et al., 2015).

Here we consider several dispersal kernels with different properties as used in Rodrigues et al. (2015), and aim to relate the thin-tailed 2D Gaussian kernel described by

$$\lambda_G(r, \theta) = \frac{1}{2\pi\sigma^2} \exp\left(-\frac{r^2}{2\sigma^2}\right) \quad (5.2)$$

and heavy-tailed kernels, when the probability distribution of moving over distance  $r$  has a power law tail, that is  $r\lambda(r, \theta) \sim r^{-\mu}$  for large  $r$ , with exponent  $\mu = 2$ . Specifically, consider the 2D Cauchy type I kernel,

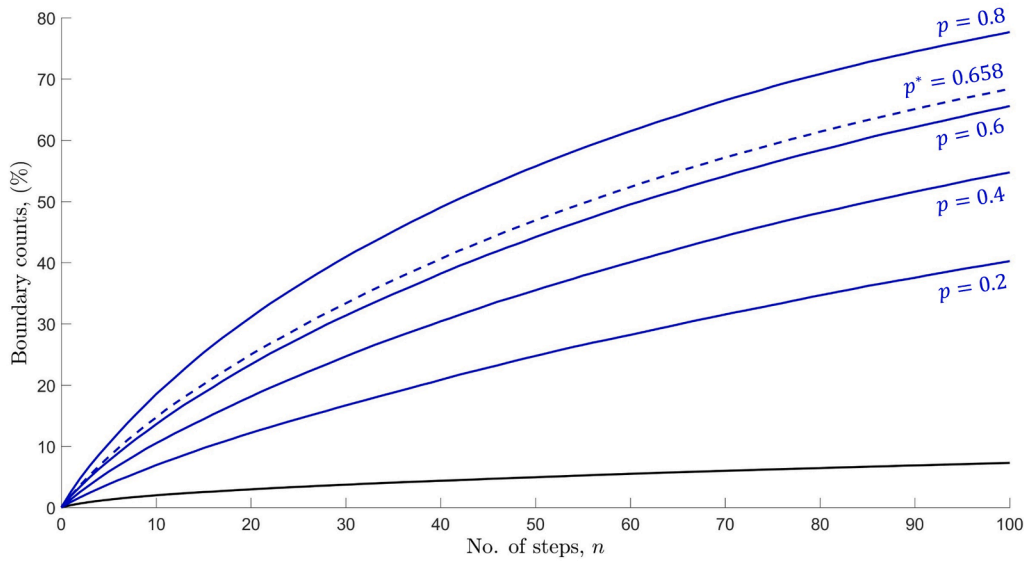


**Fig. 7.** Boundary counts computed as the proportion of individuals (%) that exit a circular region of radius  $R = 100$ , as shown in Fig. 6. The counts are recorded for a population of size  $10^5$  moving according to Brownian motion (black curve) with a Rayleigh step-length distribution ( $\sigma = 0.5$ ). Similarly, counts are also recorded for a population of the same size performing a LW (blue curves) with a folded-Cauchy step-length distribution. These step-length distributions are related with varying survival probabilities  $p = 0.2, 0.4, 0.6, 0.8$  and also for the optimal value  $p^* = 0.658$ , corresponding to  $\gamma = 0.292, 0.492, 0.696, 1.028$  and  $0.768$ , respectively. A sufficiently large population was used in the simulation run to reduce the effect of randomness in the individual movement. Each individual independently executed a walk of  $n = 100$  steps.

given by

$$\lambda_{C_1}(r, \theta) = \frac{\gamma_1}{\pi(\gamma_1 + r)^3} \tag{5.3}$$

and the 2D Cauchy type II kernel

$$\lambda_{C_2}(r, \theta) = \frac{\gamma_2}{2\pi(\gamma_2^2 + r^2)^{\frac{3}{2}}}. \tag{5.4}$$

To form a relationship between the thin- and different heavy-tailed dispersal kernels, consider the probability  $p$  of finding an individual after the dispersal exceeding a distance of radius  $a$ .

For the Gaussian kernel, we have that

$$P(r > a) = \int_0^{2\pi} \int_a^\infty \lambda_G(r, \theta) r dr d\theta = p, \tag{5.5}$$

and on computing this, we obtain the radius  $a$  as a function of  $p$ ,

$$a = \sigma \sqrt{-2 \ln p} \tag{5.6}$$

as previously seen in Eq. (3.10) for the Rayleigh probability distribution.

Similarly, for the Cauchy type dispersal kernels, we have that

$$P(r > a_i) = \int_0^{2\pi} \int_{a_i}^\infty \lambda_{C_i}(r, \theta) r dr d\theta = p, \quad i = 1, 2, \tag{5.7}$$

On evaluating this, we obtain for the Cauchy type I kernel

$$a_1 = \gamma_1 \cdot \left( \frac{\sqrt{1-p}}{1-\sqrt{1-p}} \right) \tag{5.8}$$

and for the Cauchy type II kernel

$$a_2 = \gamma_2 \cdot \frac{\sqrt{1-p^2}}{p}. \tag{5.9}$$

Given the same fixed radius in either case  $a_1 = a$  and  $a_2 = a$ , on equating (5.6) with (5.8) and (5.9) separately, we obtain a relationship between the dispersal kernel parameters as a function of  $p$ , given as

$$s_1(p) = \frac{\gamma_1}{\sigma} = \sqrt{-2 \ln p} \left( \frac{1}{\sqrt{1-p}} - 1 \right), \quad s_2(p) = \frac{\gamma_2}{\sigma} = p \sqrt{\frac{-2 \ln p}{1-p^2}}. \tag{5.10}$$

It is precisely the  $\mathbb{L}^2$ -distance between the dispersal kernels

$$\mathfrak{D}(\lambda_{C_j}, \lambda_G) = 4\pi^2 \int_0^\infty \left[ r \lambda_{C_j}(r, \theta) - r \lambda_G(r, \theta) \right]^2 dr, \quad j = 1, 2. \tag{5.11}$$

that is

$$\mathfrak{D}(\lambda_{C_1}, \lambda_G) = \frac{1}{\sigma} \int_0^\infty \left[ \frac{2s_1(p)r}{(s_1(p) + r)^3} - r \exp\left(-\frac{r^2}{2}\right) \right]^2 dr, \tag{5.12}$$

and

$$\mathfrak{D}(\lambda_{C_2}, \lambda_G) = \frac{1}{\sigma} \int_0^\infty \left[ \frac{s_2(p)r}{(s_2^2(p) + r^2)^{\frac{3}{2}}} - r \exp\left(-\frac{r^2}{2}\right) \right]^2 dr, \tag{5.13}$$

with  $\gamma_1 = \sigma s_1(p)$  and  $\gamma_2 = \sigma s_2(p)$ , that we seek to minimise to obtain an optimal probability  $p^*$ . The radius at where this occurs can be respectively determined from Eq. (5.8) and Eq. (5.9) for a fixed value of  $\sigma$ . Although the  $\mathbb{L}^2$ -distance can be written in exact form by evaluating the integrals in Eqs. (5.12)–(5.13), the expression is quite bulky and complicated (i.e., involves the Meijer G-function) and thus we resort to numerical integration. We find that the dispersal kernels are related for the Gaussian vs. Cauchy type I case with optimal probability  $p^* = 0.718$  with  $s_1 = 0.719$ ,  $a_1 = 0.814\sigma$ , and for the Gaussian vs. Cauchy type II case with  $p^* = 0.727$  with  $s_2 = 0.845$ ,  $a_2 = 0.799\sigma$ . Although we demonstrate application of our approach to the short- and long-distance dispersal kernels from Rodrigues et al. (2015) in the context of patchy invasion by stage-structured non-native species, its potential ecological implications require further exploration.

## 6. Discussion

### 6.1. Power-law distributions in animal movements

Much has been discussed in the literature regarding the existence of a power-law in the step-lengths of animal movements and the statistical approaches used to identify such distributions (Plank and Codling, 2009; Auger-Méthé et al., 2011; Plank et al., 2013). While the debate about the reality of power-law behaviour continues, observed data clearly

demonstrates traits of heavy-tailed distributions (Reynolds, 2014). Fitting power-law distributions to real-world movement data is challenging, but these distributions are useful for both mathematical analysis and biological interpretations due to their heavy tails (Edwards, 2008; Breed et al., 2015). Conversely, fitting non-power-law distributions is easier, supported by many well-developed methods. In this work, we present a method to determine the power-law distribution that most closely resembles a given non-power-law distribution, and vice versa. This approach allows for the modelling and analysis of observed movement data within both power-law and non-power-law settings, enabling direct comparisons of movement models featuring either type of distribution in step lengths. Moreover, we demonstrate that the long-distance dispersal potential of power-law distributions can be replicated by adjusting the parameter of a thin-tailed exponential distribution to match the survival probability  $p^*$ . This adjustment ensures that both distributions exhibit similar long-distance dispersal characteristics, despite their differing tail behaviours. This is useful in various ecological settings, as the diffusion capability of individual animal movement is used as a measure of dispersal capability (Bearup et al., 2016). Ecological applications are broad, including population dispersal (Gurarie et al., 2009; Hapca et al., 2009), individual interactions and contact rates (Bailey, 2023), the spread of diseases (Fofana and Hurford, 2017; Ahmed et al., 2021a), pest monitoring (Petrovskii et al., 2014; Banks et al., 2020), and foraging behaviour (Humphries et al., 2010; James et al., 2011). Below, we detail two ecological settings in which the work presented here has an immediate application.

## 6.2. Boundary counts

Boundary counts in ecology, specifically monitoring individuals exiting or entering an area, are useful for understanding population dynamics, spatial patterns, and habitat connectivity (Bearup and Petrovskii, 2015; Bearup et al., 2015; Christensen et al., 2021; Cocconi et al., 2021). For instance, in pitfall trapping used for pest monitoring, traps themselves serve as boundaries where insects are counted as they enter (Epsky et al., 2004; Petrovskii et al., 2014; Miller et al., 2015). This approach provides valuable information for improving sampling strategies, estimating population abundance and guiding control efforts (Petrovskii et al., 2012; Brown and Matthews, 2016; Engel et al., 2017; Ahmed et al., 2023). The study by Bearup et al. (2016) demonstrated that the boundary counts of *Tenebrio molitor* beetles arising from Brownian or Lévy-type movement were similar for values of the exponent  $\mu$  in the power law lying between 2.5 and 3. The implication is that the effects of the short- or long-distance dispersal becomes indistinguishable over this parameter range. In their analysis they related the normal and power-law step distributions, by fixing the value of the survival probability at  $p = 0.1$ . This was based on the empirical observation that the number of beetles leaving the arena through the external boundary in the first minute was about 10% of the total population. However, this observation can depend on the method the beetles are released into the region, it is subject to the randomness of the beetle movement, and also the proportion of exiting beetles can change on a longer time-scale. We have shown in Fig. 7 that boundary counts are indeed highly sensitive to how the distribution of step-lengths are related, specifically an increase in the survival probability leads to higher recorded counts. It follows that, to accurately infer the relationship between these distinct movement processes requires careful and considered approaches, which can depend upon the ecological context and simulation setting. Otherwise, where such information is lacking, the alternative default approach is use the optimal survival probability  $p^*$ , resulting in an objectively 'fair' comparison between the step-length distributions due to the minimisation of the dissimilarity between them. Without ecological reasoning, this approach provides a consistent, systematic method for standardising dispersal kernels, avoiding arbitrary choices.

## 6.3. Biological invasions

The introduction of non-native species is recognised as a significant threat to global ecosystems. They detrimentally impact economies (Diagne et al., 2021), the environment, and native species thereby deteriorating ecosystem functioning, which often leads to substantial biodiversity loss and human well-being (Courchamp et al., 2017). Biological invasions refer to the introduction of species, either intentionally or unintentionally, beyond their native biogeographical boundaries into areas where they have no evolutionary history. In these new environments, these species, referred to as 'non-native', may establish and potentially spread, thus becoming 'invasive' and often affecting the recipient ecosystems (Simberloff, 2013; Pyšek et al., 2020; Soto et al., 2024). This process can be conceptualised in four phases: (1) a species is intentionally or unintentionally transported to a new area through human activities, or naturally dispersing after a barrier is removed or made permeable through human action. (2) In the new region, it escapes or is willingly introduced into (evolutionary) novel locations (3) where it establishes a viable (i.e., self-sustaining) population and (4) spreads (Shigesada and Kawasaki, 1997; Blackburn et al., 2011). While the latter two stages occur with or without direct human assistance, the quality, quantity, and frequency of introductions (i.e., generally termed 'propagule pressure') are relevant at all stages (e.g., Lockwood et al., 2013; Briski et al., 2014). The concept of 'spread' in invasion ecology is therefore important because it describes to the movement and dispersal of a non-native species beyond its original point of introduction (Hui and Richardson, 2017; Wilson et al., 2008), forming the basis for the classifications of non-native populations as 'invasive' (Soto et al., 2024). Also, a better understanding of invasive spread is crucial to validating and improving theoretical models that predict spatial patterns resulting from biological invasions (Hastings, 1996; Lewis et al., 2016).

A mathematical description of the invasion process is traditionally with the application of reaction-diffusion equations (Bouin et al., 2012, 2018; Morris et al., 2019; Keenan and Cornell, 2021). Nevertheless, some have adopted an alternative framework, namely integro-difference equation (IDE) formulations, because they explicitly account for the species distinct dispersal and growth phases, and accommodate for various movement behaviours, including those exhibiting non-Gaussian characteristics (e.g., see Lutscher, 2019). In practical terms, the dispersal kernel can be determined directly through field observations, including mark-recapture, trap count, or movement data, or it can be formulated based on the fundamental physical or behavioural processes that govern movement (Skarpaas and Shea, 2007; Butikofer et al., 2018). Typical choices of the dispersal kernel that are frequently used in calculations are thin-tailed distributions such as the Gaussian or Laplace kernels (e.g., insect dispersal, Neubert et al., 1995), or where dispersal distances follow a power law decay such as the Cauchy kernel (Shaw, 1995).

Moreover, several authors have applied these IDE models to problems in invasion biology and related the dispersal kernels. For example, on investigating the patchy invasion spread of non-native species by short- and long-distance dispersal, Rodrigues et al. (2015) formulated an IDE model based on the movement of two interacting predator-prey species in 2D space. They formed a relationship between the thin- and heavy-tailed dispersal kernels by setting a radius  $a$  within which the probability of finding an individual after the dispersal is set at an arbitrary value of  $p = 0.5$ , which is the same as the probability of exceeding this distance. However, our approach improves upon this, by providing a methodology to compute the survival probability  $p^*$  based on minimising the dissimilarity between the dispersal kernels, rather than it being fixed arbitrarily. As shown in Section 5.2, we found that for the dispersal kernels considered in Rodrigues et al. (2015), in the (a) Gaussian vs. Cauchy type I case,  $p^* = 0.718$ , with ratio of dispersal kernel parameters  $s_1 = \gamma_1/\sigma = 0.719$  and characteristic radial length  $a_1 = 0.814\sigma$ , and in the (b) Gaussian vs. Cauchy type II case,  $p^* = 0.727$ ,  $s_2 = \gamma_2/\sigma = 0.845$ ,  $a_2 = 0.799\sigma$ . Contrast this to the sub-optimal relationship formed in

Rodrigues et al. (2015) with  $p = 0.5$ ,  $s_1 = (2 - \sqrt{2})\sqrt{\ln 2} \approx 0.488$ , and  $s_2 = \sqrt{(2 \ln 2)/3} \approx 0.680$ , with same radius  $a_1 = a_2 = \sigma\sqrt{2 \ln 2} \approx 1.177\sigma$ . How the pattern of invasive species spread depicted by the prey spatial distributions in Rodrigues et al. (2015) may change with these different parameter values, and what the ecological implications of these changes are, requires further analysis.

#### 6.4. Application of movement dispersal relationships given empirical data in ecological studies

A step-length distribution can be parametrised using observed movement data by analysing the distances travelled between consecutive recorded locations of an animal over time (Cagnacci et al., 2010), e.g., recording the geocoordinates of each step for ground beetles using a GPS device (Ruzickova and Elek, 2021). Each step length is measured as the straight-line distance between two successive points in the movement path. These observed step lengths can then be fitted to a statistical distribution, such as a Gaussian, exponential, or power-law distribution, depending on the movement behaviour (Breed et al., 2015; Reynolds and Ouellette, 2016; Pike and Burman, 2023). Parameter estimation is typically performed using methods like maximum likelihood estimation or Bayesian inference, ensuring that the chosen distribution best describes the observed data (Edwards, 2008; Codling and Plank, 2011; Blackwell et al., 2015). Once parametrised, the step-length distribution provides insights into the animal's movement patterns, such as the frequency of short versus long steps. This parametrisation allows the model to replicate the movement behaviour of a specific species, mimicking its real-world movement dynamics, and can inform models of animal movement in ecological studies.

To demonstrate how our approach can be applied to relate short- and long-distance movement behaviours given empirical movement data, consider the following ecological example of insect trapping. Pitfall trapping is a widely used technique to monitor ground-dwelling insects, providing insights into population abundance, species richness, and community composition (Epsky et al., 2004; Engel et al., 2017). In a simulated trapping scenario, individuals move randomly in 2D space, with traps distributed across the simulation area. Each trap has a defined boundary, and when an individual encounters this boundary, it is considered captured and removed from the system. The process repeats over time, with each trap recording the number of individuals crossing its boundary, and accumulating these counts gives the proportion of the population trapped (Petrovskii et al., 2014; Ahmed et al., 2021b, 2023). For example, consider a scenario where the movement process follows Brownian motion, and observed movement data is used to estimate the movement parameter, which governs the Rayleigh step-length distribution. Under certain conditions, such as when resources are scarce or unevenly distributed, individuals may exhibit Lévy walking behaviour, characterised by long-distance movements interspersed with frequent short steps (Reynolds et al., 2013; De Jager et al., 2014). By relating the step-length distributions under Brownian motion and Lévy walks, we gain insight into how changes in movement behaviour influence the likelihood of encountering traps and the resulting capture rates. Such analyses offer information for optimising sampling strategies, refining population estimates, and enhancing our understanding of ecological processes (Ahmed and Petrovskii, 2019).

#### 6.5. Dependency on ecological context

Animal movement in general and animal dispersal in particular are fundamental phenomena that have significant effect on many aspects of population dynamics and ecosystem functioning (Turchin, 1998; Bullock et al., 2002). Peculiarities of animal movement – in particular, whether they can be regarded as diffusive or super-diffusive – has been a focus of intense debate for almost three decades (Viswanathan et al., 2011). In spite of many questions remaining, there is sufficient evidence

that at least some of the individuals of some species can, under certain conditions, perform the movement that is better classified as super-diffusive, e.g., Lévy flights or Lévy walks, rather than diffusive, usually referred to as Brownian motion (Sims et al., 2019).

What is often forgotten in that debate is the ecological context: whatever is the movement type, what are the implications for the corresponding ecosystem and/or how does it affect the function that the given species has inside the ecological community? Super-diffusively moving animals would normally have a heavy-tailed dispersal kernel (Kot et al., 1996), which means a higher proportion of long-distance dispersers. In turn, larger dispersal distances may have a significant effect on the properties of both the given species and the ecosystem as a whole, e.g. enhancing spread of infectious diseases (Mundt et al., 2009), facilitating synchronisation between population fluctuations in different habitats (Blomfield et al., 2023), etc. There can, however, be other contexts or implications where not the forerunners but the main bulk of the population is more important. One example is given by invertebrate animals trapping for monitoring purposes, with the goal to estimate the corresponding population density (Petrovskii et al., 2012, 2014). In this case, the effect of forerunners is limited to the special case of monitoring at the edge of the advancing invasion front, i.e., where the population density is very low; however, fast dispersers hardly have any considerable effect on trap counts after the population settles down.

As another important example, there is growing evidence that animals, especially large animals, act as a vector transporting (with dung and bodies) nutrients across space, in particular phosphorus that is a limiting factor in many ecosystems (Doughty et al., 2013, 2016). Arguably, in such a case it is not the number and speed of the forerunners that matters but the typical distance that describes the movement of the bulk of the population. In turn, shifting the focus away from the forerunners has immediate implications for the choice of modelling framework. For instance, instead of more complicated modelling approaches based on integral-difference or integral-differential equations that can be sensitive to details of the dispersal kernel (which is usually difficult to restore from the data with sufficient accuracy, cf. De Jager et al. (2012), Jansen et al. (2012)), a simpler and more robust approach based on the diffusion equation can be used (Doughty et al., 2013; Bearup et al., 2016).

#### 6.6. Implications for directed movement

Since our focus is on the dispersal component of movement, we assumed there is no inherent directional preference at either a local or global scale. While this assumption is simplistic, purely random movement has proven to be a useful null model in certain cases, such as the movement of infected ants (Hughes et al., 2011). However, more realistically, most animals exhibit some degree of directional persistence, tending to maintain their trajectory over short timescales rather than making abrupt or erratic turns, with gradual adjustments being more common (Kareiva and Shigesada, 1983; Codling et al., 2008). To account for this in movement models, the orientation of successive steps is correlated (Hall, 1977; Bovet and Benhamou, 1988). RW models incorporating localised directional persistence have been widely applied to describe movement patterns across a range of taxa, from arthropods such as ants (Byers, 2001), beetles (Reynolds et al., 2013; Bailey et al., 2021; Ahmed et al., 2023), butterflies (Kareiva and Shigesada, 1983) to larger mammals like caribou (Bergman et al., 2000), providing a more ecologically realistic representation of movement dispersal. Our approach for relating purely random scale-specific and scale-free walks can also be applied in the case of localised directed movement. In this case, the step-length distributions can be related using the methodology described in this study, but would also need a means of relating the turning angle distributions. This can be achieved using the same concept of minimising the squared-Euclidean distance between the turning angle distributions, which has been used to identify mixed distributions and multiple movement behaviours in an analysis on the movements of African bull elephants (*Loxodonta Africana*) using the example case of

wrapped-normal vs. wrapped Cauchy circular distributions (Bailey and Codling, 2021).

## 7. Concluding remarks

In theoretical studies of individual animal movement, researchers often relate short- and long-distance dispersal kernels by assuming an equal survival probability  $p$ . However, the value of  $p$  is often chosen without strong ecological justification or is simply assigned arbitrarily. In contrast, we have provided a methodology to calculate a unique, optimised value for  $p$ , which ensures a more ecologically meaningful relationship between the dispersal kernels by minimising a measure of dissimilarity between them. This method addresses the shortcomings of arbitrary choices by relying on a systematic, optimisation-based approach. Moreover, we offer insights into how these choices can influence ecological dynamics. For example, when considering boundary effects, the proportion of individuals exiting a specific region can vary considerably depending on how the dispersal kernels are related. This variability underscores the critical importance of selecting  $p$  based on sound ecological reasoning or, in the absence of such reasoning, using a more rigorous and systematic comparison of dispersal kernels through the optimal survival probability. A better understanding is needed to fully grasp the broader implications of how the relationship between dispersal kernels can shape outcomes across various ecological scenarios. This should be a key area of focus for future research, where immediate applications could include investigating pitfall trap counts through simulation studies (Ahmed and Petrovskii, 2019; Petrovskii et al., 2014), exploring spatial patterns in biological invasions using the IDE framework (Lewis et al., 2016; Lutscher, 2019), and assessing contact rates between individuals in the context of disease spread (Fofana and Hurford, 2017; Bailey, 2023).

## Funding

This work was supported by Gulf University for Science and Technology (GUST) under project code ISG - Case #7 (DAA) and the European Union's Horizon Europe research and innovation programme under the Marie Skłodowska-Curie Postdoctoral Fellowship Grant Agreement No. 101203662 (PJH). The funders had no role in study design, data collection, analysis, interpretation, or decision to submit the manuscript for publication.

## CRediT authorship contribution statement

**Danish A. Ahmed:** Writing – review & editing, Writing – original draft, Visualization, Validation, Supervision, Methodology, Investigation, Funding acquisition, Formal analysis, Conceptualization; **Sergei V. Petrovskii:** Writing – review & editing, Writing – original draft; **Joseph D. Bailey:** Writing – review & editing, Writing – original draft; **Michael B. Bonsall:** Writing – review & editing, Writing – original draft; **Phillip J. Haubrock:** Writing – review & editing, Writing – original draft.

## Declaration of competing interest

The authors declare that they have no known competing financial interests or personal relationships that could have appeared to influence the work reported in this paper.

## Acknowledgements

DAA has been supported by Gulf University for Science and Technology and the Research Center CAMB under project code: ISG – Case #7. PJH is funded by the Marie Skłodowska-Curie Postdoctoral Fellowship: Grant No. 101203662.

## References

- Ahmed, D.A., Petrovskii, S.V., 2019. Analysing the impact of trap shape and movement behaviour of ground-dwelling arthropods on trap efficiency. *Methods Ecol. Evol.* 10, 1246–1264.
- Ahmed, D.A., Benhamou, S., Bonsall, M.B., Petrovskii, S.V., 2021. Three-dimensional random walk models of individual animal movement and their application to trap counts modelling. *J. Theor. Biol.* 524, 110728.
- Ahmed, D.A., Ansari, A.R., Imran, M., Dingle, K., Bonsall, M.B., 2021a. Mechanistic modelling of COVID-19 and the impact of lockdowns on a short-time scale. *PLoS One* 16, e0258084.
- Ahmed, D.A., Bailey, J.D., Petrovskii, S.V., Bonsall, M.B., 2021b. Mathematical bases for 2D insect trap counts modelling. In: Pham, T. D., Yan, H., Ashraf, M. W., Sjöberg, F. (Eds.), chapter Advances in Artificial Intelligence, Computation, and Data Science, Springer International Publishing, Cham. pp. 133–159.
- Ahmed, D.A., Beidas, A., Petrovskii, S.V., Bailey, J.D., Bonsall, M.B., Hood, A.S.C., Byers, J.A., Hudgins, E.J., Russell, J.C., Ruzickova, J., Bodey, T.W., Renault, D., Bonnaud, E., Haubrock, P.J., Soto, I., Haase, P., 2023. Simulating capture efficiency of pitfall traps based on sampling strategy and the movement of ground-dwelling arthropods. *Methods Ecol. Evol.*, 1–17.
- Andersen, M., 1991. Properties of some density-dependent integrodifference equation population models. *Math. Biosci.* 104, 135–157.
- Aspillaga, E., Safi, K., Hereu, B., Bartumeus, F., 2019. Modelling the three-dimensional space use of aquatic animals combining topography and eulerian telemetry data. *Methods Ecol. Evol.* 10, 1551–1557.
- Auger-Méthé, M., Clair, C.C.S., Lewis, M.A., Derocher, A.E., 2011. Sampling rate and misidentification of Lévy and non-Lévy movement paths: comment. *Ecology* 92, 1699–1701.
- Bailey, J., Wallis, J., Codling, E.A., 2018. Navigational efficiency in a biased and correlated random walk model of individual animal movement. *Ecology* 99 (1), 217–223.
- Bailey, J.D., Bener, C.M., Blackshaw, R.P., Codling, E.A., 2021. Walking behaviour in the ground beetle, *Poecilus cupreus*: dispersal potential, intermittency and individual variation. *Bull. Entomol. Res.* 111 (2), 200–209.
- Bailey, J.D., Codling, E.A., 2021. Emergence of the wrapped cauchy distribution in mixed directional data. *ASTA Adv. Stat. Anal.* 105, 229–246.
- Bailey, J.D., 2023. An assessment of the contact rates between individuals when movement is modelled by a correlated random walk. *Theor. Ecol.* 16, 239–252.
- Banks, J.E., Laubmeier, A.N., Banks, H.T., 2020. Modelling the effects of field spatial scale and natural enemy colonization behaviour on pest suppression in diversified agroecosystems. *Agric. For. Entomol.*, 22, 30–40.
- Bartumeus, F., Peters, F., Pueyo, S., Marrasé, C., Catalan, J., 2003. Helical Lévy walks: adjusting searching statistics to resource availability in microzooplankton. *Proc. Natl. Acad. Sci.* 100, 12771–12775.
- Bartumeus, F., Da Luz, M.G.E., Viswanathan, G.M., Catalan, J., 2005. Animal search strategies: a quantitative random-walk analysis. *Ecology* 86 (11), 3078–3087.
- Bartumeus, F., Catalan, J., 2009. Optimal search behavior and classic foraging theory. *J. Phys. A* 42 (43), 569–580.
- Bearup, D., Petrovskaya, N., Petrovskii, S., 2015. Some analytical and numerical approaches to understanding trap counts resulting from pest insect immigration. *Math. Biosci.* 263, 143–160.
- Bearup, D., Petrovskii, S., 2015. On time scale invariance of random walks in confined space. *J. Theor. Biol.* 367, 230–245.
- Bearup, D., Bener, C.M., Petrovskii, S., Blackshaw, R.P., 2016. Revisiting Brownian motion as a description of animal movement: a comparison to experimental movement data. *Methods Ecol. Evol.* 7 (12), 1525–1537.
- Benhamou, S., 2006. Detecting an orientation component in animal paths when the preferred direction is individual-dependent. *Ecology* 87 (2), 518–528.
- Benhamou, S., 2007. How many animals really do the Lévy walk? *Ecology* 88 (8), 1962–1969.
- Berg, H.C., 1983. *Random Walks in Biology*. Princeton University Press.
- Bergman, C.M., Schaefer, J.A., Luttich, S.N., 2000. Caribou movement as a correlated random walk. *Oecologia* 123 (3), 364–374.
- Blackburn, T.M., Pyšek, P., Bacher, S., Carlton, J.T., Duncan, R.P., Jarošík, V., Wilson, J.R.U., Richardson, D.M., 2011. A proposed unified framework for biological invasions. *Trends Ecol. Evol.* 26, 333–339.
- Blackwell, P.G., Niu, M., Lambert, M.S., LaPoint, S.D., 2015. Exact bayesian inference for animal movement in continuous time. *Methods Ecol. Evol.* 7 (2), 184–195.
- Blomfield, A., Menéndez, R., Wilby, A., 2023. Population synchrony indicates functional connectivity in a threatened sedentary butterfly. *Oecologia* 201, 979–989.
- Bouin, E., Calvez, V., Meunier, N., Mirrahimi, S., Perthame, B., Raoul, G., Voituriez, R., 2012. Invasion fronts with variable motility: phenotype selection, spatial sorting and wave acceleration. *C. R. Math.* 350, 761–766.
- Bouin, E., Chan, M.H., Henderson, C., Kim, P.S., 2018. Influence of a mortality trade-off on the spreading rate of cane toads fronts. *Commun. Partial Differ. Equ.* 43, 1627–1671.
- Bovet, P., Benhamou, S., 1988. Spatial analysis of animals' movements using a correlated random walk model. *J. Theor. Biol.* 131 (4), 419–433.
- Bowler, D.E., Benton, T.G., 2005. Causes and consequences of animal dispersal strategies: relating individual behaviour to spatial dynamics. *Biol. Rev.* 80, 205–225.
- Breed, G.A., Sevens, P.M., Edwards, A.M., 2015. Apparent power-law distributions in animal movements can arise from intraspecific interactions. *J. R. Soc. Interface* 12 (103), 20140927.
- Briski, E., Drake, D.A.R., Chan, F.T., Bailey, S.A., MacIsaac, H.J., 2014. Variation in propagule and colonization pressures following rapid human-mediated transport: implications for a universal assemblage-based management model. *Limnol. Oceanogr.* 59, 2068–2076.

- Brown, G.R., Matthews, I.M., 2016. A review of extensive variation in the design of pitfall traps and a proposal for a standard pitfall trap design for monitoring ground-active arthropod biodiversity. *Ecol. Evol.* 6 (12), 3953–3964.
- Bullock, J.M., Kenward, R.E., Hails, R.S., 2002. *Dispersal Ecology*. Oxford, UK: Blackwell.
- Buttkofer, L., Jones, B., Sacchi, R., Mangiacotti, M., Ji, W., 2018. A new method for modelling biological invasions from early spread data accounting for anthropogenic dispersal. *PLoS One* 13 (11). e0205591.
- Byers, J.A., 2001. Correlated random walk equations of animal dispersal resolved by simulation. *Ecology* 82 (6), 1680–1690.
- Cagnacci, F., Boitani, L., Powell, R.A., Boyce, M.S., 2010. Animal ecology meets GPS-based radiotelemetry: a perfect storm of opportunities and challenges. *Philos. Trans. R. Soc. B Biol. Sci.* 365, 2157–2162.
- Choules, J.D., Petrovskii, S., 2017. Which random walk is faster? Methods to compare different step length distributions in individual animal movement. *Math. Model. Nat. Phenom.* 12 (2), 22–45.
- Christensen, K., Cocconi, L., Sendova-Franks, A.B., 2021. Animal intermittent locomotion: a null model for the probability of moving forward in bounded space. *J. Theor. Biol.* 510 110533.
- Cleasby, I.R., Wakefield, E.D., Bearhop, S., Bodey, T.W., Votier, S.C., Hamer, K.C., 2015. Three-dimensional tracking of a wide-ranging marine predator: flight heights and vulnerability to offshore wind farms. *J. Appl. Ecol.* 52, 1474–1482.
- Clobert, J., Danchin, E., Dhondt, A.A., Nichols, J.D., 2001. *Dispersal*. Oxford University Press.
- Cocconi, L., Kuhn-Régner, A., Neuss, M., Sendova-Franks, A.B., Christensen, K., 2021. Reconstructing the intrinsic statistical properties of intermittent locomotion through corrections for boundary effects. *Bull. Math. Biol.*, 83(4) 28.
- Codling, E., Plank, M.J., Benhamou, S., 2008. Random walk models in biology. *J. R. Soc. Interface* 5 (25), 813–834.
- Codling, E.A., Plank, M.J., 2011. Turn designation, sampling rate and the misidentification of power laws in movement path data using maximum likelihood estimates. *Theor. Ecol.* 4.3 (2011), 397–406.
- Codling, E.A., Bode, N.W.F., 2016. Balancing direct and indirect sources of navigational information in a leaderless model of collective animal movement. *J. Theor. Biol.* 394, 32–42.
- Cooper, N., Sherry, T., Marra, P.P., 2014. Modeling three-dimensional space use and overlap in birds. *Auk* 131, 681–693.
- Courchamp, F., Fournier, A., Bellard, C., Bertelsmeier, C., Bonnaud, E., Jeschke, J.M., Russell, J.C., 2017. Invasion biology: specific problems and possible solutions. *Trends Ecol. Evol.* 32 (1), 13–22.
- De Jager, M., Weissing, F.J., Herman, P.M.J., Nolet, B.A., van de Koppel, J., 2012. Response to comment on “Lévy walks evolve through interaction between movement and environmental complexity”. *Science* 335 (6071), 918.
- De Jager, M., Bartumeus, F., Kölzsch, A., Weissing, F.J., Hengeveld, G.M., Nolet, B.A., Herman, P.M.J., Van De Koppel, J., 2014. How superdiffusion gets arrested: ecological encounters explain shift from Lévy to Brownian movement. *Proc. R. Soc. B Biol. Sci.* 281, 20132605.
- De Knegt, H.J., Hengeveld, G.M., Van Langevelde, F., De Boer, W.F., Kirkman, K.P., 2007. Patch density determines movement patterns and foraging efficiency of large herbivores. *Behav. Ecol.* 18, 1065–1072.
- Diagne, C., Leroy, B., Vaissière, A.C., Gozlan, R.E., Roiz, D., Jarić, I., Salles, J.M., Bradshaw, C.J.A., Courchamp, F., 2021. High and rising economic costs of biological invasions worldwide. *Nature* 592, 571–576.
- Doughty, C.E., Wolf, A., Malhi, Y., 2013. The legacy of the pleistocene megafauna extinctions on nutrient availability in amazonia. *Nat. Geosci.* 6, 761–764.
- Doughty, C.E., Roman, J., Faurby, S., et al., 2016. Global nutrient transport in a world of giants. *Proc. Natl. Acad. Sci. USA* 113 (4), 868–873.
- Edwards, A., 2008. Using likelihood to test for Lévy flight search patterns and for general power-law distributions in nature. *J. Anim. Ecol.* 77 (6), 1212–1222.
- Ellis, J., Petrovskaya, N.B., Petrovskii, S., 2018. Effect of density-dependent individual movement on emerging spatial population distribution: Brownian motion vs. Lévy flights. *J. Theor. Biol.* 464, 159–178.
- Engel, J., Hertzog, L., Tiede, J., Wagg, C., Ebeling, A., Briesen, H., Weisser, W.W., 2017. Pitfall trap sampling bias depends on body mass, temperature, and trap number: insights from an individual-based model. *Ecosphere* 8, e01790.
- Epsky, N.D., Morrill, W.L., Mankin, R., 2004. Traps for capturing insects. In: *Encyclopedia of Entomology*. Springer, Dordrecht.
- Fofana, A.M., Hurford, A., 2017. Mechanistic movement models to understand epidemic spread. *Philos. Trans. R. Soc. B Biol. Sci.* 372, 20160086.
- Grimm, V., Railsback, S., 2005. *Individual-Based Modeling and Ecology*. Princeton University Press.
- Gurarie, E., Anderson, J.J., Zabel, R.W., 2009. Continuous models of population-level heterogeneity inform analysis of animal dispersal and migration. *Ecology* 90, 2233–2242.
- Gurarie, E., Ovaskainen, O., 2013. Towards a general formalization of encounter rates in ecology. *Theor. Ecol.* 6, 189–202.
- Hall, R.L., 1977. Amoeboid movements as a correlated walk. *J. Math. Biol.* 4, 327–335.
- Hapca, S., Crawford, J.W., Young, I.M., 2009. Anomalous diffusion of heterogeneous populations characterized by normal diffusion at the individual level. *J. R. Soc. Interface* 6, 111–122.
- Hastings, A., 1996. Models of spatial spread: a synthesis. *Biol. Conserv.* 78, 143–148.
- Holmes, E.E., Lewis, M.A., Banks, J.E., Veit, R.R., 1994. Partial differential equations in ecology: spatial interactions and population dynamics. *Ecology* 75, 17–29.
- Hooten, M.B., Johnson, D.S., McClintock, B.T., Morales, J.M., 2017. *Animal Movement: Statistical Models for Telemetry Data*. CRC Press, Boca Raton. first ed.
- Hughes, D.P., Andersen, S.B., Hywel-Jones, N.L., Himaman, W., Billen, J., Boomsma, J.J., 2011. Behavioral mechanisms and morphological symptoms of zombie ants dying from fungal infection. *BMC Ecol.*, 11 (1), 13.
- Hui, C., Richardson, D.M., 2017. *Invasion Dynamics*. Oxford University Press. first ed.
- Humphries, N.E., Queiroz, N., Dyer, J.R., Pade, N.G., Musyl, M.K., Schaefer, K.M., et al., 2010. Environmental context explains Lévy and Brownian movement patterns of marine predators. *Nature* 465 (7301), 1066–1069.
- Humphries, N.E., Weimerskirch, H., Queiroz, N., Southall, E.J., Sims, D.W., 2012. Foraging success of biological Lévy flights recorded in situ. *Proc. Natl. Acad. Sci.* 109, 7169–7174.
- James, A., Plank, M.J., Edwards, A.M., 2011. Assessing Lévy walks as models of animal foraging. *J. R. Soc. Interface* 8 (62), 1233–1247.
- Jansen, V.A.A., Mashanova, A., Petrovskii, S., 2012. Comment on “Lévy walks evolve through interaction between movement and environmental complexity”. *Science* 335(6071) 918.
- Kareiva, P.M., 1983. Local movement in herbivorous insects: applying a passive diffusion model to mark-recapture field experiments. *Oecologia* (Berlin) 56(234).
- Kareiva, P.M., Shigesada, N., 1983. Analyzing insect movement as a correlated random walk. *Oecologia* 56 (2–3), 234–238.
- Kawai, R., Petrovskii, S.V., 2012. Multiscale properties of random walk models of animal movement: lessons from statistical inference. *Proc. R. Soc.* 468, 1428–1451.
- Keenan, V.A., Cornell, S.J., 2021. Anomalous invasion dynamics due to dispersal polymorphism and dispersal-reproduction trade-offs. *Proc. R. Soc. B Biol. Sci.* 288 20202825.
- Kot, M., Schaffer, W.M., 1986. Discrete-time growth-dispersal models. *Math. Biosci.* 80, 109–136.
- Kot, M., Lewis, M.A., van den Driessche, P., 1996. Dispersal data and the spread of invading organisms. *Ecology* 77, 2027–2042.
- Lewis, M., Neubert, M., Caswell, H., Clark, J., Shea, K., 2006. A guide to calculating discrete-time invasion rate from data. chapter Cadotte, M.W., McMahon, S.M., Fukami, T., (Eds.), *Conceptual Ecology and Invasion Biology: Reciprocal Approaches to Nature*, Springer, pp. 69–192.
- Lewis, M.A., Petrovskii, S.V., Potts, J.R., 2016. *The mathematics behind biological invasions*. Interdisciplinary Applied Mathematics, Springer International Publishing, Cham.
- Lin, C.C., Segel, L.A., 1974. *Mathematics Applied to Deterministic Problems in the Natural Sciences*. New York, NY: Macmillan.
- Lockwood, J.L., Hoopes, M.F., Marchetti, M.P., 2013. *Invasion Ecology*. Wiley-Blackwell, Chichester. second ed.
- Lutscher, F., 2019. Integro-difference equations in spatial ecology. *Interdisciplinary Applied Mathematics*, Springer International Publishing, Cham.
- Miller, J.R., Adams, C.G., Weston, P.A., Schenker, J.H., 2015. *Trapping of small organisms moving randomly*. Principles and applications to pest monitoring and management. Springer Briefs in Ecology. United States: Springer.
- Morris, A., Börger, L., Crooks, E., 2019. Individual variability in dispersal and invasion speed. *Mathematics* 7, 795.
- Mundt, C.C., Sackett, K.E., Wallace, L.D., Cowger, C., Dudley, J.P., 2009. Long-distance dispersal and accelerating waves of disease: empirical relationships. *Am. Nat.* 173 (4), 456–466.
- Nathan, R., Getz, W.M., Revilla, E., Holyoak, M., Kadmon, R., Saltz, D., 2008. A movement ecology paradigm for unifying organismal movement research. *Proc. Natl. Acad. Sci. USA* 105, 19052–19059.
- Neubert, M.G., Kot, M., Lewis, M.A., 1995. Dispersal and pattern formation in a discrete-time predator-prey model. *Theor. Pop. Biol.* 48, 7–43.
- Nolet, B.A., Mooij, W.M., 2002. Search paths of swans foraging on spatially autocorrelated tubers. *J. Anim. Ecol.* 71, 451–462.
- Okubo, A., 1980. *Diffusion and Ecological Problems: Mathematical Models*. Springer, Berlin.
- Okubo, A., Levin, S.A., 2001. *Diffusion and Ecological Problems: Modern Perspectives*. Berlin, Germany: Springer.
- Petrovskii, S., Morozov, A., 2009. Dispersal in a statistically structured population: fat tails revisited. *Am. Nat.* 173 (2), 278–289.
- Petrovskii, S., Bearup, D., Ahmed, D.A., Blackshaw, R., 2012. Estimating insect population density from trap counts. *Ecol. Complex.* 10, 69–82.
- Petrovskii, S., Petrovskaya, N., Bearup, D., 2014. Multiscale approach to pest insect monitoring: random walks, pattern formation, synchronization and networks. *Phys. Life Rev.* 11 (3), 467–525.
- Pike, T.W., Burman, O.H.P., 2023. Simulating individual movement in fish. *Sci. Rep.* 13, 14581.
- Plank, M.J., Codling, E.A., 2009. Sampling rate and misidentification of Lévy and non-Lévy movement paths. *Ecology* 90, 3546–3553.
- Plank, M.J., Auger-Méthé, M., Codling, E.A., 2013. *Lévy or Not? Analysing Positional Data from Animal Movement Paths*. Springer, Berlin, Heidelberg. 2071.
- Pyšek, P., Hulme, P.E., Simberloff, D., Bacher, S., Blackburn, T.M., Carlton, J.T., Dawson, W., Essl, F., Foxcroft, L.C., Genovesi, P., Jeschke, J.M., Kühn, I., Liebhold, A.M., Mandrak, N.E., Meyerson, L.A., Pauchard, A., Pergl, J., Roy, H.E., Seebens, H., Van Kleunen, M., Vilà, M., Wingfield, M.J., Richardson, D.M., 2020. Scientists’ warning on invasive alien species. *Biol. Rev.* 95, 1511–1534.
- Reynolds, A.M., 2010. Bridging the gulf between correlated random walks and Lévy walks: autocorrelation as a source of Lévy walk movement patterns. *J. R. Soc. Interface* 7, 1753–1758.
- Reynolds, A.M., Leprêtre, L., & Bohan, D.A., 2013. Movement patterns of tenebrio beetles demonstrate empirically that correlated-random-walks have similitude with a Lévy walk. *Sci. Rep.* 3 (1), 3158.
- Reynolds, A.M., 2014. Mussels realize weierstrassian Lévy walks as composite correlated random walks. *Sci. Rep.* 4 (1), 4409.
- Reynolds, A.M., Ouellette, N.T., 2016. Swarm dynamics may give rise to Lévy flights. *Sci. Rep.* 6 30515.
- Reynolds, A.M., 2018. Current status and future directions of Lévy walk research. *Biol. Open*. 7 (1), bio030106.

- Rodrigues, L., Mistro, D., Cara, E., Petrovskaya, N., Petrovskii, S., 2015. Patchy invasion of stage-structured alien species with short-distance and long-distance dispersal. *Bull. Math. Biol.* 77 (8), 1583–1619.
- Ruzickova, J., Elek, Z., 2021. Recording fine-scale movement of ground beetles by two methods: potentials and methodological pitfalls. *Ecol. Evol.* 11 (13), 8562–8572.
- Sandefur, J., 2018. A unifying approach to discrete single-species populations models. *Discrete Contin. Dyn. Syst. - Ser. B* 23, 493–508.
- Shaw, M.W., 1995. Simulation of population expansion and spatial pattern when individual dispersal distributions do not decline exponentially with distance. *Proc. R. Soc. Lond. B Biol. Sci.* 259, 243–248.
- Shigesada, N., Kawasaki, K., 1997. *Biological Invasions: Theory and Practice*. Oxford University Press, Oxford.
- Simberloff, D., 2013. *Invasive Species: What Everyone Needs to Know*. Oxford University Press, first ed.
- Sims, D.W., Humphries, N.E., Hu, N., Medan, V., Berni, J., 2019. Optimal searching behaviour generated intrinsically by the central pattern generator for locomotion. *eLife* 8 e50316.
- Skarpaas, O., Shea, K., 2007. Dispersal patterns, dispersal mechanisms, and invasion wave speeds for invasive thistles. *Am. Nat.* 170 (3), 421–430.
- Skellam, J.G., 1973. The formulation and interpretation of mathematical models of diffusionary processes in population biology. In: Bartlett, M. S., Hiorns, R. W. (Eds.), in: *The Mathematical Theory of the Dynamics of Biological Populations* Edition. pp. 63–85.
- Soto, I., Balzani, P., Carneiro, L., Cuthbert, R.N., Macedo, R., Tarkan, A.S., Haubrock, P.J., et al., 2024. Taming the terminological tempest in invasion science. *Biol. Rev. brv*.13071.
- Tracey, J., Sheppard, J., Zhu, J., Wei, F., Swaisgood, R., Fisher, R., 2014. Movement-based estimation and visualization of space use in 3d for wildlife ecology and conservation. *PLoS One* 9 (7). e101205.
- Turchin, P., 1998. *Quantitative analysis of movement. Measuring and Modelling Population Redistribution in Animals and Plants*. Sinauer Associates, Inc., Sunderland, Massachusetts.
- Viswanathan, G., Afanasyev, V., Buldryrev, S., Havlin, S., Luz, d., Raposo, M., Stanley, H., 2000. Levy flights in random searches. *Physica* 282, 1–12.
- Viswanathan, G., Afanasyev, V., Buldryrev, S., Havlin, S., da Luz, M.G.E., Raposo, M., Stanley, H., 2011. *The Physics of Foraging*. Cambridge University Press.
- Williams, H.J., Taylor, L.A., Benhamou, S., Bijleveld, A.I., Clay, T.A., de Grissac, S., Demšar, U., English, H.M., Franconi, N., Gómez-Laich, A., Griffiths, R.C., Kay, W.P., Morales, J.M., Potts, J.R., Rogerson, K.F., Rutz, C., Spelt, A., Trevail, A.M., Wilson, R.P., Börger, L., 2020. Optimising the use of biologgers for movement ecology research. *J. Anim. Ecol.* 89, 186–206.
- Wilson, R.P., Shepard, E.L., Liebsch, N., 2008. Prying into the intimate details of animal lives: use of a daily diary on animals. *Endang. Species. Res.* 4, 123–137.
- Zurell, D., Berger, U., Cabral, J.S., Jeltsch, F., Meynard, C.N., Münkemüller, T., Nehrbaas, N., Pagel, J., Reineking, B., Schröder, B., Grimm, V., 2010. The virtual ecologist approach: simulating data and observers. *Oikos* 119, 622–635.